Modelling of corium stratification in the lower plenum of a reactor vessel

M. Salay , F. Fichot *

Institut de RadioProtection et de Sûreté Nucléaire - IRSN -
Département de Recherches en Sécurité,
B.P.3 - 13115 Saint Paul Lez Durance, France.

Abstract

A comprehensive modelling to predict the stratification of oxides and metals in a corium pool is presented. It consists of a series of models that take into account both thermochemical and thermalhydraulic aspects. The model is designed to be used on a 2D/3D meshing. Therefore, the corium pool is assumed to be non-homogeneous in temperature and composition. Only local thermochemical equilibrium is assumed (in each mesh).
A simplified thermochemical model provides the equilibrium compositions of the oxide and metal phases. It is consistent with MASCA experimental results. It is also consistent with computational results obtained by using IRSN thermochemical database. All the local physical properties, and particularly the densities, are calculated from the local compositions and temperature.
The relative motion of the two phases is calculated with a drift flux model. This provides the velocities of the materials in the pool and, therefore, the global transport of species. Fission products are also transported, assuming, for each fission product, a pre-defined local equilibrium distribution between oxide and metal phases.
The model is implemented in a test-version of ICARE/CATHARE V2.0, a severe accident code developed by IRSN. Comparisons of the code results with selected MASCA tests show a good agreement. The OECD MASCA program was dedicated to the study of the thermochemical interactions between typical corium materials in a molten pool. A one-dimensional transient with successive steel additions is presented to demonstrate the existence of a transient "3-layer" configuration. In such configurations, the oxide pool is surrounded by two metallic layers with different compositions. It corresponds to a global non-equilibrium situation which may remain for a significant time, depending on species transport processes across the oxide pool. A reactor configuration used to study the effects of the progressive melting of lower plenum steel structures in a two-dimensional corium pool is also presented.

*Corresponding author. Email : florian.fichot@irsn.fr , Fax : (33) 4.42.25.64.68

Nomenclature

Roman letters

d diameter, m
f absolute fraction
h enthalpy, J.kg^{-1}
m mass, kg
M molar mass, kg.mol^{-1}
n mole fraction
N quantity, mol
p pressure, N.m^{-2}
S saturation, $S = \varepsilon_\ell/\varepsilon$
t time, s
T temperature, K
x mass fraction
v velocity, m.s^{-1}
V volume, m^3

Greek symbols

α volume fraction of liquid
Δt time step, s
μ viscosity, N.s.m^{-2}
ν concentration fraction
λ thermal conductivity, W.m^{-1}.K^{-1}
ρ density, kg.m^{-3}
ε volume fraction, porosity, $\varepsilon = 1 - \varepsilon_\mathrm{s}$
σ surface tension, N.m^{-1}

Subscripts

b buoyant
$k\phi$ 'k' in phase 'ϕ'
$k\phi\xi$ 'k' in 'ϕ' considering only ξ
$kn\xi$ 'k' when there is no ξ
$j \pm \mathrm{n}$ mesh index, n = 0 or 1
$j \pm 1/2$ mesh face index
k element or species index
ℓ liquid
m metal
s sinking
s solid
t terminal
x oxide

Superscripts

n previous time step
$n+1$ current time step
$+$ positive component
$-$ negative component

Overscripts

$\rightarrow$ vector

1 Introduction

1.1 Background

In case of a hypothetical severe accident in a pressurized water reactor (PWR), the destruction of fuel rods and melting of materials lead to the accumulation of core materials, commonly called "debris", in the lower plenum of the reactor vessel. The debris may be partially solid and liquid, with a molten pool surrounded by solid particles. The heat flux across the vessel wall becomes higher when the size of the molten pool increases. Many experimental studies, such as COPO, ACOPO, BALI, RASPLAV-SALT and SIMECO, have dealt with the problem of heat flux distribution around a volumetrically heated pool. All those experiments were conducted with simulant materials with the aim of reaching a high Rayleigh number comparable to the case of a large molten pool in the reactor pressure vessel (RPV) lower head. The objective has been to determine whether the imposed heat flux would not exceed the heat removal capability (critical heat flux) on the external surface of the vessel. The heat-focusing effect of a molten metal layer was considered as an important cause for vessel failure because the vessel walls adjacent to the metal layer would be subjected to increased heat fluxes. Up to now, the concept of in-vessel retention by external cooling has been investigated by several countries for different reactor designs (existing or future concepts), assuming that the metal layer would be on top of the oxidic pool. This corresponds to what we may call the "standard analysis".

1.2 The standard analysis

Thermalhydraulic studies of melt pool behavior have also included cases where a molten metal (steel) layer could form on top of oxidic corium due to very limited solubility of steel in the oxides (the density of steel being lower than the density of core oxides). Scoping calculations have confirmed that shallow metal layers located on top of the oxide pool may produce heat fluxes at the adjacent walls that could exceed the critical heat flux under certain conditions [24]. Moreover vessel wall thinning reduces the margins of allowable mechanical loads. Studies of the impact of materials have been performed in the frame of OECD RASPLAV project. It demonstrated that the homogeneous corium melt behaved comparably to simulant materials in natural circulation, therefore previous evaluations based on simulant material data could be scaled to prototypic reactor conditions. It was shown that such a behavior can be expected if the molten pool contained only oxidic materials. However, some RASPLAV results and the first MASCA results indicated that the behavior of the corium molten pool likely depends upon its composition and Zirconium oxidation degree and a non-miscible metallic layer may be located either on top or at the bottom of the oxidic pool. In light of these results the interest was to obtain more data with respect to prototypic core materials behavior at high temperatures.

1.3 Miscibility gap and stratification

Indeed, the existence of a miscibility gap between two liquids in the U-Zr-Fe-O diagram makes the situation more complex than assumed in the earlier studies. MASCA results have confirmed earlier assumptions that the metal phase could actually be heavier than the oxide pool. The first consequence is that it is necessary to derive models that are able to deal with both situations (metal above or under) and possible transitions between situations. The second consequence is that it is not possible to consider the different phases present in the lower plenum (solid debris or crusts, oxide pool, metal pool) as chemically independent. Any modelling of the solidification and stratification processes in the debris must include a thermochemical sub-model, as it was earlier mentioned by Seiler and Froment [18] and in Fichot *et al.* [10]. For fission products, a similar approach is necessary to predict their distribution in the pool. In MASCA experiments, it was observed that the fission product partitioning between the oxide and metal phases is consistent with what can be calculated with current thermochemical databases. The consequence is that a significant amount of residual power may be released in the metallic phase. Hence, the volumetric power in the oxide would be lower than before its interaction with steel. This was usually not considered in previous analyses.
It appears necessary to evaluate and gather in a comprehensive model all the relevant phenomena that occur in a molten pool in the lower plenum of a PWR. Even if not aiming at in-vessel retention, there is a clear need to understand the convective molten pool behavior, since melt pools have important implications on the core relocation and the RPV failure mode that both, in turn, have further consequences on the subsequent behavior of corium outside the vessel, which depends strongly on the melt composition and ejection mode.

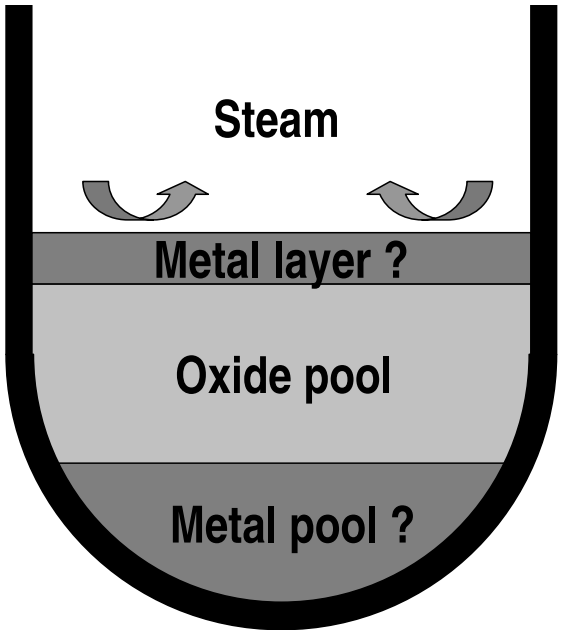

Fig. 1: Three layer schematic representation

In this paper, we derive a multi-dimensional model for metal-oxide stratification in a molten pool. The model includes a thermochemical database that is used to predict the local equilibrium compositions. The model is implemented in the ICARE/CATHARE code which is a mechanistic code developed by IRSN and devoted to the calculation of severe accident scenarios in PWRs, [13]. Some consequences of the stratification process are shown. In particular, it is demonstrated that transient situations involving three layers (a top metallic layer, the oxidic pool and a heavy bottom metallic layer) are likely to exist if there are successive additions of steel into the corium pool, Fig. 1. Such configurations actually correspond to a global thermochemical non-equilibrium and they are not likely to exist in steady state. However, such configurations may remain long enough to lead to an increased heat flux across the top metallic layer and possible vessel failure, which cannot be predicted by the "standard" steady-state analysis.

2 Modelling of the miscibility gap

2.1 Main trends observed in MASCA results and earlier studies

In a series of small and middle scale tests performed in the MASCA program with Iron and stainless steel, there is a migration of metallic Zirconium and Uranium from suboxidized corium towards the metallic phase (initially steel), leading to the increase of metallic phase mass and density and consequently to a possible change of layer configuration. This phenomenon seems to be very important for the in-vessel and ex-vessel melt behaviour and for accident management procedures. Precise measurements of the temperature and the composition of metallic and oxidic phases provided important data for validation of thermodynamic databases. It is clear that Uranium transport to the metallic phase is closely related to the existence of free Zirconium in the initial suboxidized corium. The amounts of U and Zr atoms transferred to the metallic phase also seem to be proportional to the ratio of added steel mass to the initial corium mass. A very small amount of Iron goes into the oxidic phase (less than 1% wt.). After interaction, the degree of oxidation of the oxidic phase is increased. Increasing the steel to corium ratio leads to increase the oxidic phase oxidation, approaching complete oxidation.

2.2 A fast equilibrium model based on thermochemical calculations

Implementing a Gibbs energy solver instead of the simple model is not currently reasonable for a meshed system given the computational time requirements.
For that reason the general modelling approach is to approximate the tie lines predicted by the IRSN thermochemical database using Fe, Ni, and Cr in relative concentrations corresponding to those of the average of the MA-1 and MA-2 tests. Steel behavior was taken to be the average behavior of Fe, Ni, and Cr. Several sets of assumptions were used to implement different levels of approximation. These are referred to as the base model and the miscibility limit model. The base model relates Oxygen content in the oxidic phase to steel content in the metallic phase. The aspect of the tie line approximation that differed from those predicted by the IRSN thermochemical database

was the U/Zr separation between phases. The U/Zr ratio was kept as constant, initially for simplicity, and subsequently because this assumption led to a good prediction of the MASCA results. The metallic phase concentrations were taken as those where the tie line intersects the U-Zr-steel plane whereas the oxidic phase concentrations were taken as those where the tie line intersects the U-Zr-O plane. While the prediction of Uranium and Zirconium fractions in the metallic phase were reasonable, using these points on the tie line allowed no Oxygen in the metallic phase and no steel in the oxidic phase. While this may, at first glance, seem reasonable this behavior is not consistent with the IRSN thermochemical database or the MASCA experiments, both of which predicted Oxygen in the metallic phase and steel in the oxidic phase. Oxygen in the metallic phase would reduce its overall density thus changing the concentrations at which buoyancy inversion occurs. In the case of low steel content, it is necessary to properly account for steel migration to the oxidic phase as it may comprise a significant fraction of the initial steel content. If this is not done significant errors may occur in the prediction of the total phase mass. For fixed U, Zr, and steel concentrations in the metallic phase (the primary comparison parameters for phase separation in the MASCA tests) the total metallic phase mass (closely related to the metal layer thickness in the case of a buoyant metallic phase) are linearly dependent on the fraction of steel mass lost to the oxidic phase. An additional adverse effect of using these points as the metallic and oxidic phase concentrations was that all mixtures were immiscible, even when the mixture contained solely U, Zr, and O in concentrations that should clearly be miscible. Due to these important effects miscibility limits were added to the model which are fits to those predicted by the IRSN thermochemical database. The metallic phase concentrations are taken to be those at the intersection of the tie line with the metallic phase miscibility surface while the oxidic phase concentrations are taken to be those at the intersection of the tie line with the oxidic phase miscibility surface. Due to the miscibility limits miscible mixtures can be predicted.

2.2.1 Assumptions

- The separation behavior is assumed independent of temperature because minimal changes in the equilibrium concentrations are predicted by the IRSN thermochemical database.
- The assumed order of oxygen affinity within a phase is U, then Zr (allows for UO_2 and Zr to coexist).
- In ICARE steel is considered as an individual material instead of a mixture of Fe, Ni, and Cr. As a result, steel was likewise considered for the model.
- Steel (Fe,Ni,Cr) oxides are not considered.
- The enthalpy of reaction (chemical separation) is negligible.
- The concentration of Oxygen when the tie line is extended until no steel is present has a linear relationship with the concentration of steel when the tie line is extended until no Oxygen is present.

- The behavior of the concentration of Oxygen and steel is independent of the U/Zr ratio. Very little change was observed in calculations using the IRSN thermochemical database.
- The oxidic and metallic phases have the same U/Zr ratio.

The separation equations are presented in appendix A.

2.3 Model assessment on MASCA

The MASCA experiments were primarily assessed on the metallic phase Uranium and Zirconium mass fractions. The relative masses of the metallic and oxidic phases were also used as assessment parameters. The model input parameters were not readily available from data. Some processing was required which is described below.

2.3.1 Input mole fraction determination

The phase separation model uses element number fractions as input. However a conversion is required as only the following parameters are available in Bechta [4]:

- The Uranium to Zirconium mole ratio - '$F = n_U/n_{Zr}$'
- The metallic phase mass fraction - 'x_{steel}'
- The mole fraction of Oxygen to Uranium and Zirconium combined - '$O\Sigma = n_O/(n_U + n_{Zr})$'

Values for these parameters for the MASCA tests presented in Bechta [4] are shown in Table 1. Using these three parameters and the molar masses from the ICARE database, the mole fractions, $n_U, n_O, n_{Zr}, n_{steel}$, of the entire mixture are determined. These mole fractions were then used as inputs for the separation model with the results compared to data.
The conversion from parameters given in Bechta [4] to element number fractions was performed as follows for each test:
First, the n_U/n_{Zr} mole ratio, F, is converted to mole fraction, $\mathrm{xu} = n_U/(n_U + n_{Zr})$ by:

$$\mathrm{xu} = \frac{\mathrm{F}}{1+\mathrm{F}} \tag{1}$$

Then the Oxygen, Uranium, and Zirconium number fractions in pre-steel-addition corium are calculated by:

$$n_{O,corium} = \frac{O\Sigma}{1+O\Sigma} \tag{2}$$

$$n_{U,corium} = (1 - n_{O,corium})\mathrm{xu} \tag{3}$$

$$n_{Zr,corium} = (1 - n_{O,corium})(1 - \mathrm{xu}) \tag{4}$$

Table 1: MASCA Parameters, from Bechta [4]

Test	$n_O/(n_U + n_{Zr})$	n_U/n_{Zr}	x_{steel}
MA-1	1.45	1.5	0.122
MA-2	1.77	1.3	0.114
MA-3	1.36	1.1	0.118
STFM-2	1.45	1.2	0.019
STFM-3	1.36	1.1	0.018
STFM-4	1.34	1.1	0.045
STFM-5	1.38	1.1	0.016
STFM-6	1.5	1.2	0.018
STFM-7	1.58	1.2	0.017
STFM-8	1.97	1.6	0.018
STFM-9	1.29	1.1	0.098
STFM-14	1.56	1.1	0.156
STFM-15	1.35	1.3	0.091

The mass fractions in pre-steel-addition corium are then calculated from the corium number fractions and the molar masses in the following manner:

$$\begin{aligned} m_{t,corium} &= n_{O,corium}M_O + n_{U,corium}M_U \\ &+ n_{Zr,corium}M_{Zr} \quad (5) \\ \mathrm{x}_{O,corium} &= n_{O,corium}M_O/m_{t,corium} \quad (6) \\ \mathrm{x}_{U,corium} &= n_{U,corium}M_U/m_{t,corium} \quad (7) \\ \mathrm{x}_{Zr,corium} &= n_{Zr,corium}M_{Zr}/m_{t,corium} \quad (8) \end{aligned}$$

where M is the molar mass.
The total mixture Oxygen, Uranium, and Zirconium mass fractions can then be calculated:

$$\begin{aligned} \mathrm{x}_O &= \mathrm{x}_{O,corium}(1 - \mathrm{x}_{steel}) \quad (9) \\ \mathrm{x}_U &= \mathrm{x}_{U,corium}(1 - \mathrm{x}_{steel}) \quad (10) \\ \mathrm{x}_{Zr} &= \mathrm{x}_{Zr,corium}(1 - \mathrm{x}_{steel}) \quad (11) \end{aligned}$$

Finally total mixture steel, Oxygen, Uranium, and Zirconium mole fractions are calculated:

$$\begin{aligned} N_t &= \mathrm{x}_{steel}/M_{steel} + \mathrm{x}_O/M_O + \mathrm{x}_U/M_U \\ &+ \mathrm{x}_{Zr}/M_{Zr} \quad (12) \\ n_{steel} &= (\mathrm{x}_{steel}/M_{steel})/N_t \quad (13) \\ n_O &= (\mathrm{x}_O/M_O)/N_t \quad (14) \\ n_U &= (\mathrm{x}_U/M_U)/N_t \quad (15) \\ n_{Zr} &= (\mathrm{x}_{Zr}/M_{Zr})/N_t \quad (16) \end{aligned}$$

Table 2: Calculated MASCA element mole fractions

Test	n_U	n_{Zr}	n_O	n_{steel}
MA-1	0.203	0.135	0.491	0.171
MA-2	0.175	0.134	0.547	0.144
MA-3	0.186	0.169	0.483	0.162
STFM-2	0.217	0.181	0.576	0.027
STFM-3	0.216	0.197	0.561	0.026
STFM-4	0.210	0.190	0.536	0.064
STFM-5	0.215	0.196	0.567	0.023
STFM-6	0.213	0.177	0.585	0.025
STFM-7	0.207	0.172	0.598	0.023
STFM-8	0.202	0.127	0.648	0.023
STFM-9	0.197	0.179	0.485	0.138
STFM-14	0.164	0.149	0.488	0.200
STFM-15	0.209	0.161	0.500	0.130

These calculated 'element' number fractions, shown for the MASCA tests in Table 2, were then used as inputs for the separation model.
The MA-1 and MA-2 input element number fractions were checked against values which are given for these two tests in Asmolov *et al.* [1]. This also serves to verify the method used to calculate these input element mole fractions. The system element mole fraction values of 0.20232, 0.13921, 0.49687, 0.16160 for MA-1 and 0.17451, 0.13598, 0.55200, 0.13751 for MA-2 for U, Zr, O, and steel, respectively, given in Asmolov *et al.* [1] are consistent with the values calculated using parameters given in Bechta [4] which are shown in Table 1.

2.3.2 Separation model comparison with data

Both the element mass fractions in the metallic phase and the phase mass fractions are compared against data. While the mass fractions in the metallic phase were compared against all experiments the phase mass fractions were initially compared only against the MA-1 through MA-3 experiments as this parameter was only available for this test series at the time.
Reasonable agreement has been observed overall between the miscibility limit model for both species mass fractions within a phase and for the relative phase masses.

2.3.3 Mass fractions in metallic phase

The predicted Uranium and Zirconium mass fractions in the metallic phase are compared with data presented in Bechta [4] for all experiments. Oxygen in the metallic phase was ignored for the purposes of this calculation. The measurement of Oxygen content is very difficult.

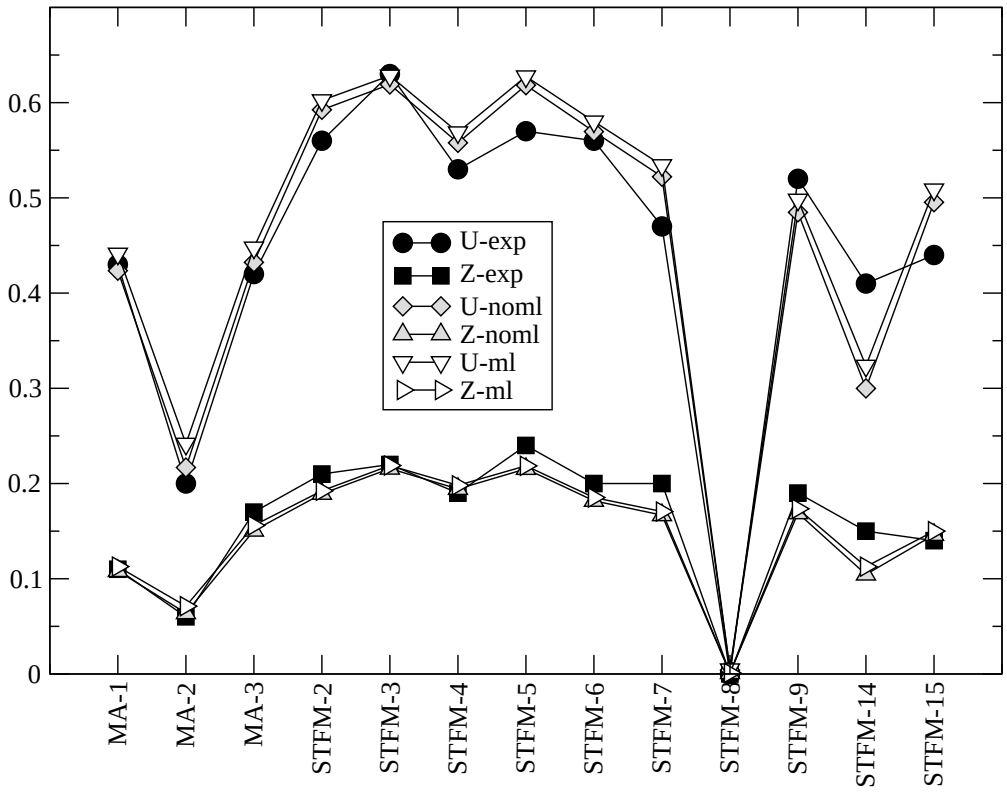

Fig. 2: Comparisons of metallic phase mass fractions with MASCA data

Table 3 compares the metallic phase mass fractions predicted by the base model with data. Other than underpredictions for both Uranium and Zirconium in STFM-14 experiment, which has the highest steel content, the separation model predicts phase separation reasonably well. These comparisons were made with the base model. With the addition of the miscibility limits, the model predicts slightly higher metallic phase mass fractions of both Uranium and Zirconium, Fig 2. In the legend *'exp'* denotes experiment, *'noml'* represents the base model with no miscibility limits, and *'ml'* designates the updated model with miscibility limits.
Similar U and Zr mass fractions are given in the metallic phase for the MA-1 and MA-2 tests in Asmolov *et al.* [1]: 0.43159 U, 0.10473 Zr for MA-1 and 0.20215 U, 0.0552 Zr for the MA-2 test. These are consistent with values found in Bechta [4].
The STFM-Fe consists of STFM tests 2, 3, 4, 5, 9, 14, and 15 along with MA tests 1 and 3. Overall, the Zirconium mass fraction is well predicted. However the Uranium mass fraction data is not as well reproduced. Moreover the Uranium mass fraction in the metallic phase is overpredicted much of the time resulting in the prediction of a more dense metallic phase and different global concentrations at which density inversion

Table 3: Comparison of base model predicted and experimental species mass fractions in metallic phase

	Experiment		Model	
test	x_U	x_{Zr}	x_U	x_{Zr}
MA-1	0.43	0.11	0.424	0.108
MA-2	0.20	0.06	0.217	0.064
MA-3	0.42	0.17	0.432	0.151
STFM-2	0.56	0.21	0.593	0.189
STFM-3	0.63	0.22	0.619	0.216
STFM-4	0.53	0.19	0.558	0.194
STFM-5	0.57	0.24	0.618	0.215
STFM-6	0.56	0.20	0.570	0.182
STFM-7	0.47	0.20	0.522	0.167
STFM-8	0	0	0.004	0.001
STFM-9	0.52	0.19	0.485	0.169
STFM-14	0.41	0.15	0.300	0.104
STFM-15	0.44	0.14	0.495	0.146

occurs. Both the Uranium and Zirconium mass fractions in the metallic phase are underpredicted for the STFM-14 test - the one with the highest steel content.
The metallic phase mass fractions for high steel mass fractions are generally well predicted by the model. For lower mass fraction cases the Uranium mass fraction in the metallic phase is overpredicted while the Zirconium mass fraction in the metallic phase is underpredicted. This further highlights the fact that the U/Zr ratio is not always the same for both phases for low steel mass fractions.
Fig 3 shows a similar comparison for mole fractions for the data presented in the MASCA summary draft report [17]. The Fe tests correspond to the STFM tests in Fig 2. The labels used were the same as those given by the sources. The element mass fractions within each phase were available from the MASCA summary draft report [17] in addition to the parameters provided in Bechta [4]. The total composition, used as input for the separation model, was determined by multiplying the element mass fractions in each phase by that phase's mass and adding the masses of each element in both phases together resulting in the total mass of each element in the molten mixture. The steel mass was considered to be the sum of masses of Fe, Ni, and Cr. FP simulant masses were ignored. The model agreement with data is not as good as that for the data presented in Bechta [4] even for the same experiments. The need for a U/Zr model is illustrated in this figure where the predicted ratio between Uranium and Zirconium in the metal phase has a much greater spread than the nearly equal data mole fractions. If the initial Oxygen concentrations were determined in a similar manner as done with the data from Bechta [4], the match may be improved.

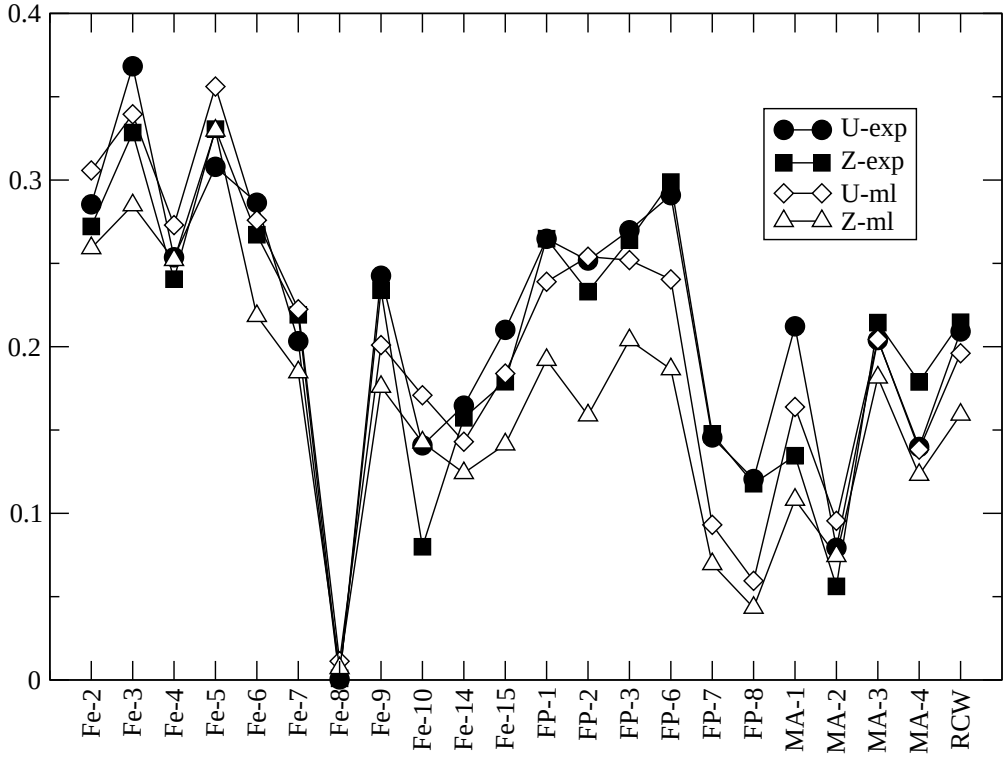

Fig. 3: Comparisons of miscibility limit model predicted metallic phase mole fractions with MASCA data

2.3.4 Relative phase masses

The relative phase mass is a parameter which can be used to determine relative phase quantities, and therefore the thickness of an upper metal layer, if present.
The predicted and experimental phase mass fractions are shown in Table 4. Data for the MA-1 and MA-2 tests are calculated using values given in Asmolov *et al.* [1] while data for the MA-3 test is calculated from values given in Bechta [4].
Allowing steel into the oxidic phase would lower the total metallic phase mass as the quantity of Uranium and Zirconium is proportional to the mass of steel in the metallic phase.
Even though the Fe content represented less than 2% of the oxidic phase (both by mass and mole), between 10 and 20% of Fe ended up in the oxidic phase for the MA-1 and MA-2 test data provided in Asmolov *et al.* [1]. If this amount of steel were allowed in the oxidic phase in the model, the predicted metallic phase mass would be reduced proportionally.

Data for the relative metallic and oxidic phase masses were recently made available in the MASCA draft summary report [17]. It allows the comparison of this parameter to the model. Figure 4 shows the comparison of the of the experimental values of metal phase mass fraction with predictions by the miscibility limit model. As expected, the better the prediction of Uranium and Zirconium fractions in the metal phase the better the prediction of the metal phase mass fractions.

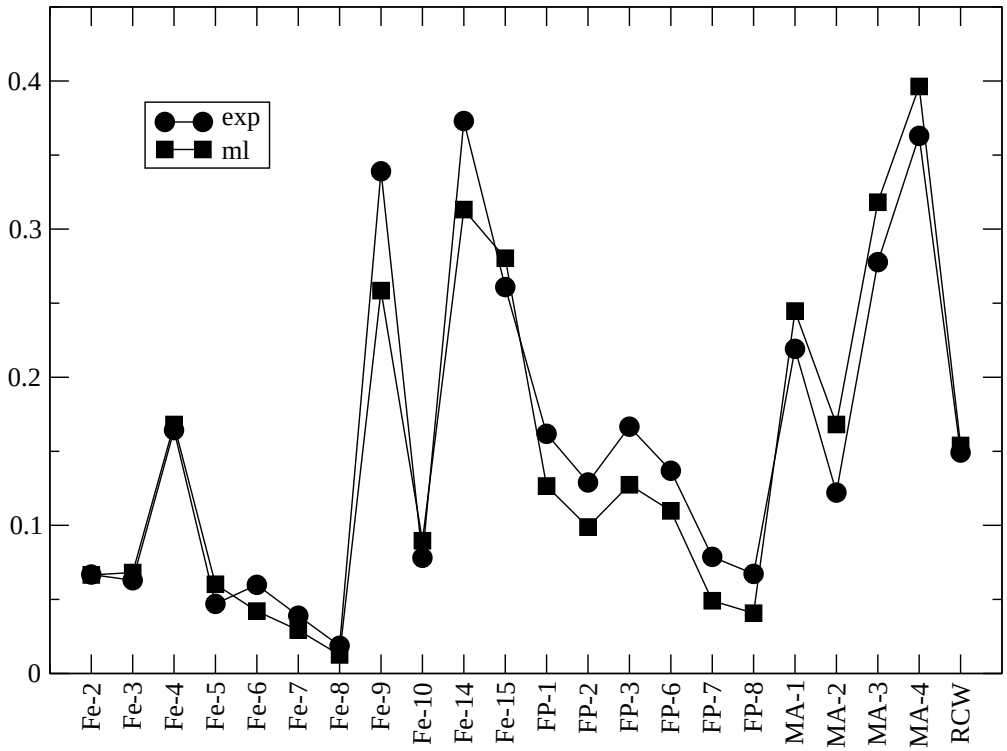

Fig. 4: Metallic phase mass fraction comparison with MASCA data

2.3.5 Separation model behavior

Figs 5, 6, 7, and 8 show the miscibility limits predicted by the separation model . Figs 5, 6, and 7 show the bounding cases while Fig 8 shows the behavior for a U/Zr ratio of 1.2. When the U/Zr ratio is held constant for both phases, the tie lines fall on the U/Zr = constant planes. This can be seen on the UZO figure (Fig. 7). Fig 8 uses a parameter, 'q', which represents U+Zr in the ratio specified.

Table 4: Comparison of predicted and experimental phase mass fractions

	Experiment		Model	
test	x_{metal}	x_{oxide}	x_{metal}	x_{oxide}
MA-1	0.781	0.219	0.739	0.261
MA-2	0.878	0.122	0.842	0.158
MA-3	0.722	0.278	0.717	0.283

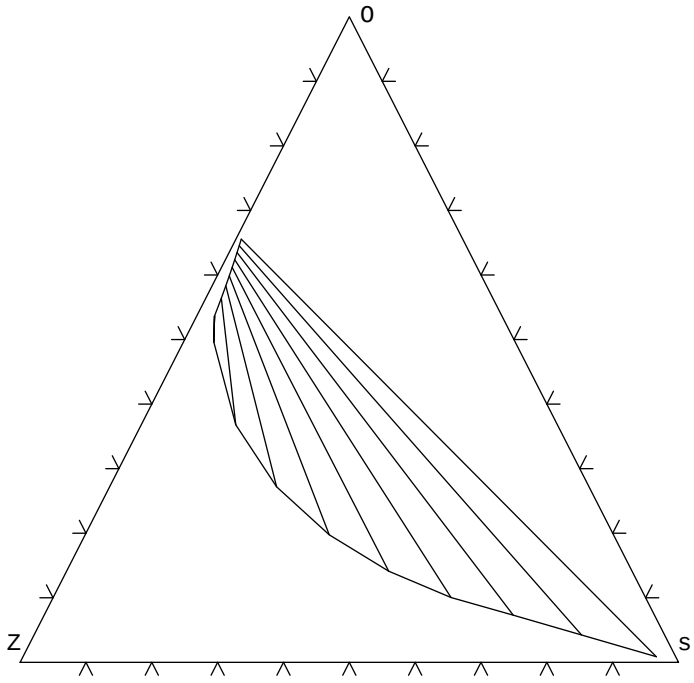

Fig. 5: Model miscibility behavior Zr-O-steel plane

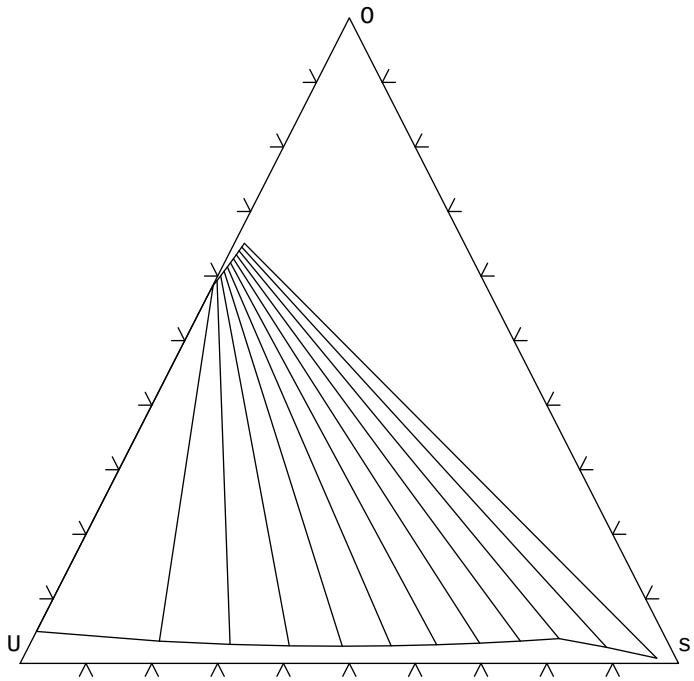

Fig. 6: Model miscibility behavior U-O-steel plane

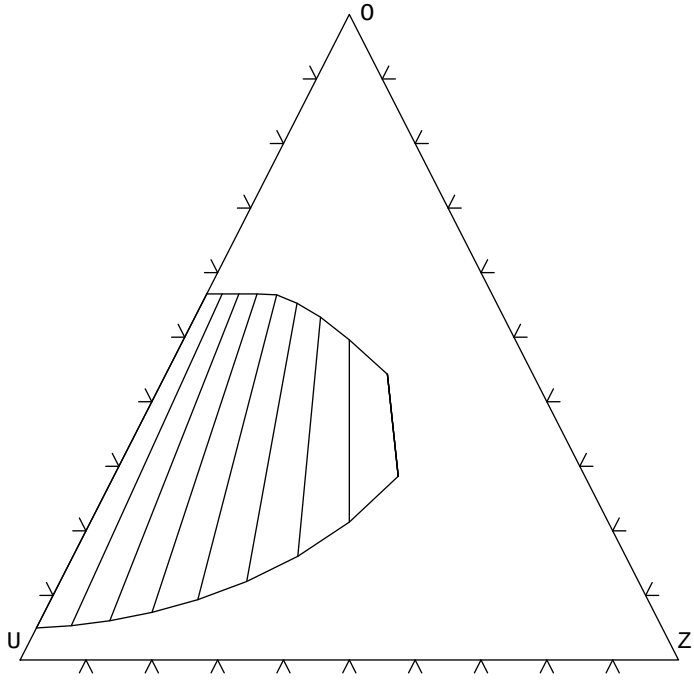

Fig. 7: Model miscibility behavior U-Zr-O plane

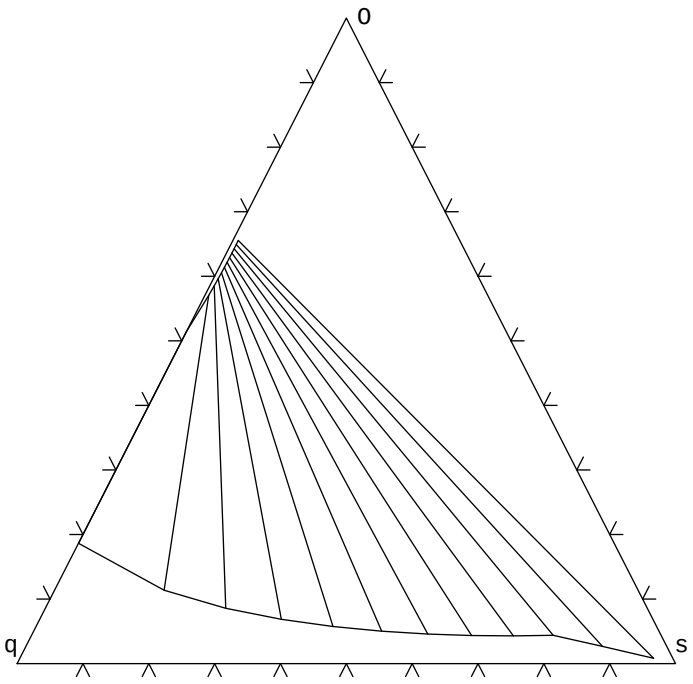

Fig. 8: Model miscibility behavior U/Zr = 1.2

2.3.6 Potential model modifications

Current work is underway to improve the method for determining the U/Zr partitioning between phases (currently $\mathrm{U/Zr}|_{\mathrm{metal}} = \mathrm{U/Zr}|_{\mathrm{oxide}}$). Preliminary calculations strongly suggest that for most tests a significant improvement can be made in predictions of the MASCA data presented in Bechta [4].
Recalculating the fits using data instead of results of the IRSN thermochemical database is not expected to significantly improve the match between model results and data.

3 Calculation of liquid phase densities

3.1 Models for densities

Densities are calculated for each species using the following equation:

$$\rho_{k,T} = A_k - B_k \times (T - T_{k0}) \tag{17}$$

where A_k, B_k, and T_{k0} are specific to each species. The used coefficients and densities evaluated at 2800K are as given in table 5.

- UO_2 values are averages of the Drotning [9], Christensen [6], Breitung [5], and Harding [14] models
- ZrO_2 values are those of the Rasplav model [8]

Table 5: Species density coefficients

	A	B	T_0(K)	$\rho_{T=2800\text{K}}$
UO_2	8775	0.913875	3120	8884.7
ZrO_2	5150	0.445	2983	5152.4
Fe	7075	1.10725	1808	5755.2
U	17428.25	1.361375	1408	15261.0
Zr	6240	0.29	2128	5987.1

- Fe values are averages of the Kirschenbaum [12], Benedicks, Lucas, and Iida [16] models
- U values are averages of the Grosse [12], Rohr [23], Mulford [20], and Fischer [11] models
- Zr values are those of the Paradis model [21]

Phase specific material properties, P, for each phase, ϕ, are determined by mass fraction weighting over the sum of species, 'k' as follows:

$$P_{\text{av.}} = \frac{\sum_k \mathrm{x}_{k\phi} P_k}{\sum_k \mathrm{x}_{k\phi}} \tag{18}$$

In the specific case of densities (inverse specific volume) this becomes:

$$\rho_{\text{av.}} = \frac{\sum_k \mathrm{x}_{k\phi}}{\sum_k \frac{\mathrm{x}_{k\phi}}{\rho_k}} \tag{19}$$

3.2 Application to an AP-600-like configuration

Some advanced reactor designs include, based on the assumption of a two layer corium configuration with a buoyant steel-only metallic phase, sufficient steel in the lower regions of the vessel so that, in the event of a severe accident involving core relocation to the lower head, the molten steel layer will be thick enough to reduce the focussing effect to the extent that the critical heat flux on the outside of the vessel wall will not be exceeded [25] [19] [15]. But the possibility of "trapping" steel at the bottom of the vessel changes such conclusions as mentionned by Rempe *et al.* [22]. It may be assumed that, for low quantities of molten steel, the inital metallic phase would include enough Zirconium and Uranium to make it heavier than the oxide pool. Then, as steel is added to corium, the equilibrium metallic phase could become lighter. The evolutions of the metal and oxide densities are represented in Fig. 9, for a corium composition corresponding to the AP600. This reactor was chosen for convenience because many analyses of in-vessel retention for the AP600 have already been presented, and many data and results are available. The purpose of this example is obviously not to change earlier conclusions, but to bring up new considerations that might help for further analysis of the in-vessel retention concept. In Fig. 9, it can be observed that there

exists a threshold value of the mass of steel, above which the equilibrium metallic phase becomes buoyant. This value depends on the oxygen potential of the corium. For a fully oxidized corium, the metallic phase will always be buoyant and mainly made of steel. Because of the progressive melting of materials and the large size of the pool, the global equilibrium can only be considered as a simplified representation. The actual process is more likely to lead to temporary configuration with three layers (light metal, oxide, heavy metal). The details of the transient processes will be described in section 5. Such results show that, for suboxidized corium, even for a large total mass of molten steel, a thin metallic layer may form on top of the oxide pool and induce a high heat flux on the vessel wall while the remaining steel lies at the bottom of the vessel.

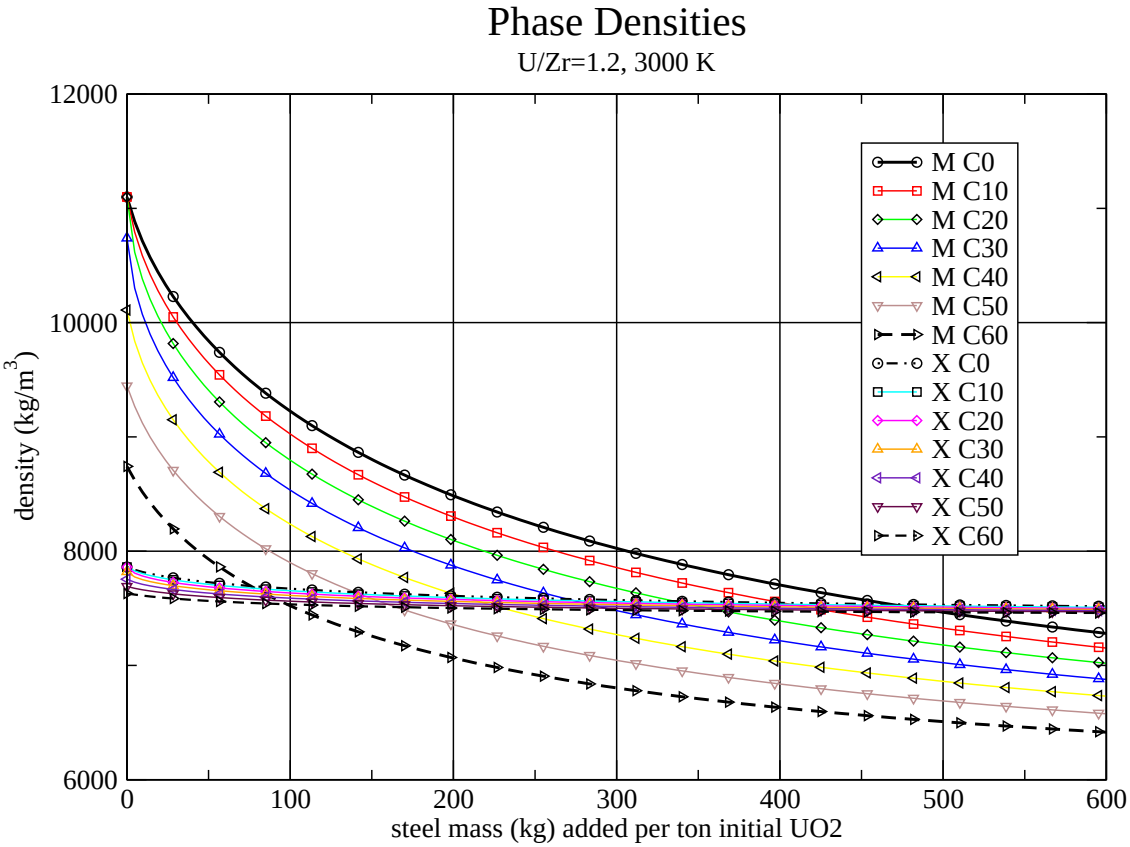

Fig. 9: Phase density calculations for a 1.2 U/Zr mole ratio at 3000K(M = metal, X = Oxide, Cx = oxidized fraction of Zr)

4 Modeling of stratification

In the present formulation, the transport due to phase separation is done separately from the bulk transport (natural circulation) and the mixing transport (turbulent/laminar

species diffusion). This allows the phase transport to be calculated with a fixed spatial discretization based on an assumption that the drift transport velocities are much greater than those of the bulk flow.

4.1 Momentum transfer : a drift model

Assumptions in the phase transport model:

- terminal velocity, u_t, stays constant throughout time step
- phase properties stay constant throughout time step
- the two non-miscible phases are treated as continuous media.

An interesting aspect of the two-phase-transport model is that the buoyant phase is not necessarily the same for the entire geometry and instead is determined on a mesh by mesh basis. The current implicit formulation of transport performs very well and can even function in situations where meshes contain liquid volumes that differ by several orders of magnitude as may occur when the liquid level in a mesh is very low or when solid materials begin to melt in a mesh.

4.2 Species transport

The volume fraction of the buoyant phase is solved for

$$\frac{\partial \alpha_b}{\partial t} + \frac{\partial u_b \alpha_b}{\partial z} = 0 \tag{20}$$

discretized as:

$$\frac{\alpha_{b,j}^{n+1} - \alpha_{b,j}^{n}}{\Delta t} + \frac{1}{V_{\ell,j}} \left(A_{j+1/2} u_{b,j+1/2}^{n+1} \alpha_{b,j}^{n+1} - A_{j-1/2} u_{b,j-1/2}^{n+1} \alpha_{b,j-1}^{n+1} \right) = 0 \tag{21}$$

The buoyant velocity, u_b, is always positive.
The net contribution of drift to volumetric flow is zero. As the drift flow is considered to be larger than bulk flow (the bulk flow is calculated separately) volumetric fluxes of each phase across any face are equal and opposite, the buoyant drift velocities at the mesh interface '$j + 1/2$' can be described as:

$$u_{b,j+1/2} = \frac{u_{t,j+1/2}}{1 + \frac{\rho_{l,j} x_{b,j} \rho_{s,j+1}}{\rho_{l,j+1} x_{s,j+1} \rho_{b,j}}} = u_{t,j+1/2} \frac{(1 - \alpha_{b,j+1})}{1 + \alpha_{b,j} - \alpha_{b,j+1}} \tag{22}$$

The sinking velocity for the same face is then:

$$u_{s,j+1/2} = u_{b,j+1/2} - u_{t,j+1/2} \tag{23}$$

The formulation for the buoyant velocity is substituted into eq 21 using new time $(n+1)$ values for the buoyant velocity.

The resulting equation that is solved for:

$$\frac{\alpha_{b,j}^{n+1}-\alpha_{b,j}^{n}}{\Delta t}+\frac{1}{V_{\ell,j}}\left(A_{j+1/2}u_{t,j+1/2}^{n}\frac{\alpha_{b,j}^{n+1}(1-\alpha_{b,j+1}^{n+1})}{1+\alpha_{b,j}^{n+1}-\alpha_{b,j+1}^{n+1}}\right.$$
$$\left.-A_{j-1/2}u_{t,j-1/2}^{n}\frac{\alpha_{b,j-1}^{n+1}(1-\alpha_{b,j}^{n+1})}{1+\alpha_{b,j-1}^{n+1}-\alpha_{b,j}^{n+1}}\right) = 0 \quad (24)$$

The buoyant and sinking phases are identified for each mesh 'j' as follows:

$$\mathrm{x}_{mbb} = 0.5+0.5(\vec{u}_t)/|\vec{u}_t| \quad (25)$$
$$\mathrm{x}_{xbb} = 1-\mathrm{x}_{mbb} \quad (26)$$

The fraction x_{mbb} is 1 when u_t is positive (i.e. the metallic phase is buoyant), and 0 when u_t is negative (i.e. metallic phase sinks)
The buoyant and sinking phase properties are calculated for mesh 'j' as follows:

$$\mathrm{x}_b = \mathrm{x}_m\mathrm{x}_{mbb}+\mathrm{x}_x\mathrm{x}_{xbb} \quad (27)$$
$$\rho_b = \rho_m\mathrm{x}_{mbb}+\rho_x\mathrm{x}_{xbb} \quad (28)$$
$$\mathrm{x}_s = \mathrm{x}_m\mathrm{x}_{xbb}+\mathrm{x}_x\mathrm{x}_{mbb} \quad (29)$$
$$\rho_s = \rho_m\mathrm{x}_{xbb}+\rho_x\mathrm{x}_{mbb} \quad (30)$$

For each mesh face involved in vertical flow, the terminal velocity is the average of the magnitude of the terminal velocities of the meshes on either side calculated as:

$$u_{t,j+1/2} = 0.5(|\vec{u}_{t,j}|+|\vec{u}_{t,j+1}|) \quad (31)$$

Face terminal velocities are always positive while the sign of the mesh terminal velocity indicates the metallic phase flow direction for that mesh. Terminal velocities were used explicitly. The terminal velocity may change somewhat as the equilibrium phase concentrations change due to sources or sinks or an originally non-uniform (and also not in equilibrium) species distribution. The terminal velocity may also change somewhat as separation progresses if the initial mixture is non-uniform or if sources or sinks of materials are present (e.g. melting, solidification, pouring in). However, it is assumed that the local composition does not change rapidly.

4.3 Determination of terminal velocity

The terminal velocity is adapted from a model presented in Clift *et al.* [7] for contaminated systems of single drops in infinite media which is considered to be valid for Morton numbers such that $\mathrm{M} < 10^{-3}$, Eötvös number such that $\mathrm{Eo} < 40$, and Reynolds numbers such that $\mathrm{Re} > 0.1$. These conditions are generally in the cases of interest for us.
This model was chosen to compensate somewhat for the potential presence of surfactants in the mixture as it relates measured single phase measured properties (future

surfactants are evenly distributed within the fluid and do not greatly effect surface tension) to two phase behavior (surfactants initially evenly distributed within each phase collect at the interface between the two).
The following assumptions were made for the terminal velocity:

- There is no assumed dispersed phase, thus drops of oxide in continuous metal and drops of metal in continuous oxide are simultaneously considered with the resulting terminal volume fraction being volume fraction weighted.
- The liquid is infinite.
- Dispersed flow behaves similar to a drop in infinite liquid.
- No wall effects were considered.
- drop size is limited by the ratio of surface tension to buoyancy forces and not by turbulence
- multiple drop effects are not considered

The terminal velocities for each phase assuming each is the dispersed phase are calculated as follows:

$$u_{t,m} = \frac{\mu_x}{\rho_x d_m} \mathrm{M}_m^{-0.149} (\mathrm{J}_m - 0.857) \tag{32}$$

$$u_{t,x} = \frac{\mu_m}{\rho_m d_x} \mathrm{M}_x^{-0.149} (\mathrm{J}_x - 0.857) \tag{33}$$

with the final mesh terminal velocity is then taken as:

$$u_t = (u_{t,m}\alpha_x + u_{t,x}\alpha_m)/\mu_r \tag{34}$$

where μ_r is the relative viscosity which takes into account possible solid debris particles flowing with the corium.
The entire listing of equations involved in the calculation of the terminal velocity is given in appendix B.

4.3.1 Modeling of turbulent mixing

For the moment the turbulent diffusivity is user provided. In a future step, the value will be taken to be equal to the turbulent thermal diffusivity already calculated in ICARE on the assumption that the turbulent Sc is equal to the turbulent Pr.
For each species and fission product, 'k', diffusion, which is the first transport step performed, is calculated as:

$$\frac{\partial \phi_k}{\partial t} - \mathrm{D_k} \nabla^2 \phi_k = 0 \tag{35}$$

where ϕ_k is the mass per unit volume of species 'k' and $\mathrm{D_k}$ is the diffusion coefficient.

4.4 Fission product separation

Fission products are transported using a pre-defined local equilibrium distribution between oxidic and metallic phases for each fission product. The partitioning coefficients for several fission products (concentration of FP in metallic phase/concentration of FP in oxidic phase) were available in MASCA data given in Asmolov *et al.* [2]. The fractional concentration, $\nu_{k,m}$, was defined such that, for a given fission product, $\nu_{k,m}/(1-\nu_{k,m})$ returns the partitioning coefficient for that fission product. The fraction of a given fission product in the control volume that resides in each phase is calculated using $\nu_{k,m}$ as follows:

$$\mathrm{f}_{k,m} = \frac{\mathrm{x}_m \nu_{k,m}}{\mathrm{x}_m \nu_{k,m} + (1-\mathrm{x}_m)(1-\nu_{k,m})} \tag{36}$$

$$\mathrm{f}_{k,x} = 1 - \mathrm{f}_{k,m} \tag{37}$$

For fission products which wre not available in the thermochemical ddatabase, analogies were made with fission products belonging to the same chemical group, as presented in Baichi [3]. Some fission products can also be allowed to exhibit the same separation behavior as either Uranium or Zirconium. In this case $\mathrm{f}_{k,m}$ is considered to be the same as for the element it is associated with. e.g. the phase separation of fission products associated with Uranium would be calculated by:

$$\mathrm{f}_{k,m} = \frac{\mathrm{x}_{um}}{\mathrm{x}_{um} + \mathrm{x}_{ux}} \tag{38}$$

Once the association of FPs with phase has been made, the same method for transport is used as for species' mass and energy.

5 1D applications

To qualify the behavior on the simplest geometry 1D tests were performed. An increased diffusion coefficient was used to simulate bulk flow recirculation and turbulent mixing. The 1D geometry consists of a region with a height of 1.2m which was separated into 20 equal divisions. The system is adiabatic. Two general cases were studied: an originally uniform mixture of UO2, ZrO2, steel, and Zr and an originally uniform mixture of UO2, ZrO2, and Zr with steel poured in from above. Very small quantities of fission products were added to observe the fission product separation behavior (mostly) independent of a heat source.

For an initially uniform mixture, it is not necessary to model turbulent species diffusion to calculate the final stratified state. The final composition of the two layers is the same as that predicted by applying the separation model to the entire system mass. Without the diffusion model activated, this is true only for an originally uniform mixture with no subsequent mass addition,

But for cases with a localized steel injection, if turbulent diffusion was not activated, the species concentration within a phase would not equilibrate and a Uranium rich metal layer would rest on the bottom while a steel only metal layer would stay on top. The addition of species diffusion allowed species in the oxidic phase to equilibrate, resulting

in a net upward transfer of free Zirconium to the upper interface with the steel only layer allowing U and Zr to migrate across that interface. This case is presented in more details in the next subsection.

5.1 Transient application with inversion of stratification

The presented 1D transient calculation consists of an originally steel-free corium mixture subjected to two steel injections, the first resulting in a negatively buoyant equilibrium metallic phase and the second resulting in a buoyant equilibrium metallic phase. Following each injection and until the equilibrium state is reached a 3-layer metal-oxide-metal configuration exists.
The predicted residence time of an unstable 3-layer configuration is inversely proportional to the effective diffusion coefficient which is the expected result for a standard diffusion process. The rate of the inversion process is limited by the transport of free Zr in the oxidic phase to and from the metal/oxide interfaces. Figs 10 and 11 show the species profiles at different times in the transient while Fig 12 shows the steel mass fraction history at different levels. The meshing divisions are shown in the profile plots. The four times were selected for the profile plots to show two 3-layer configurations each followed by its equilibrium 2-layer configuration. The first equilibrium concentrations following the initial steel injection results in a heavier metallic phase while the equilibrium concentrations following the second injection result in a buoyant metallic phase.

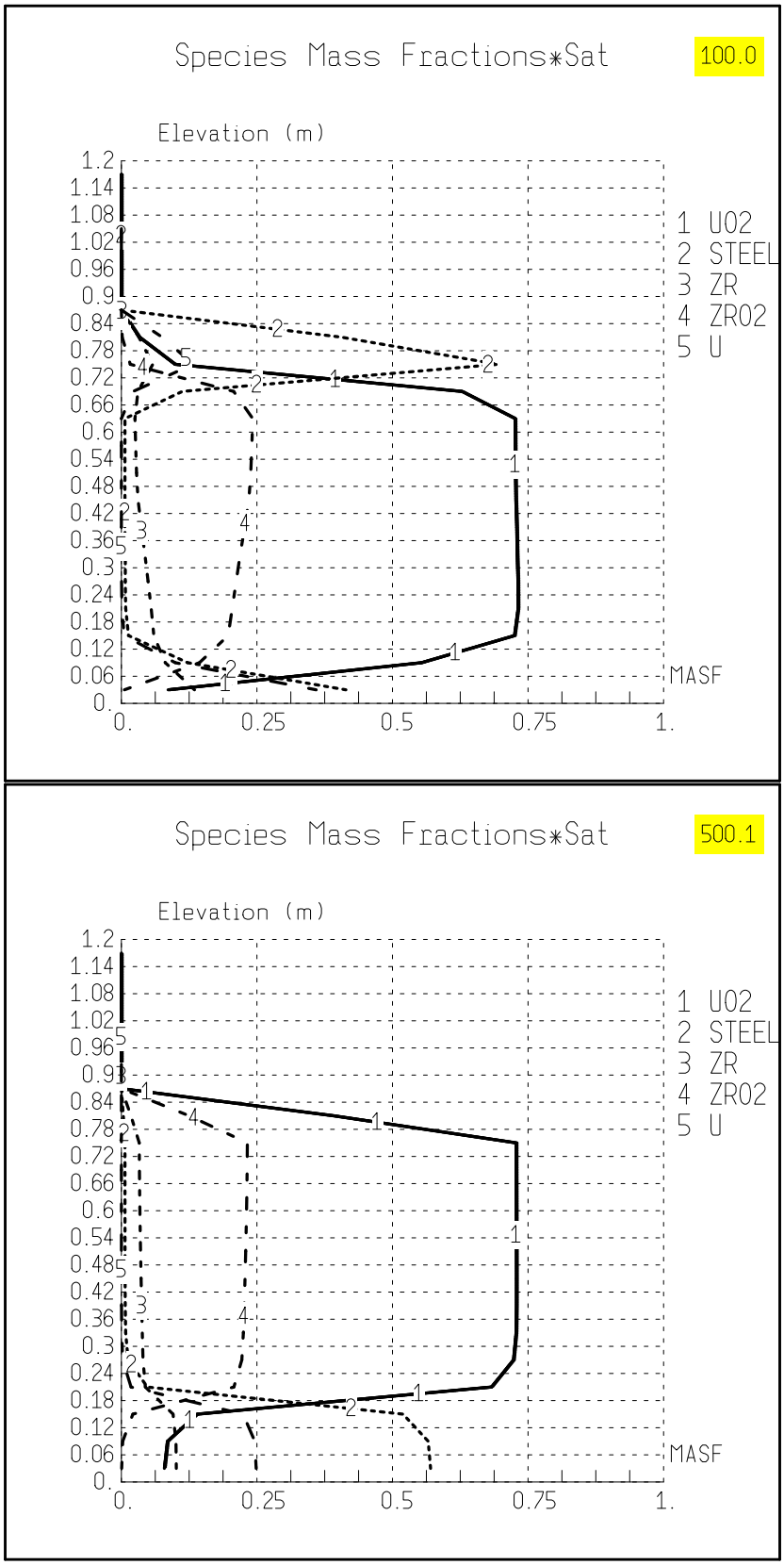

Fig. 10: Species concentration profiles A

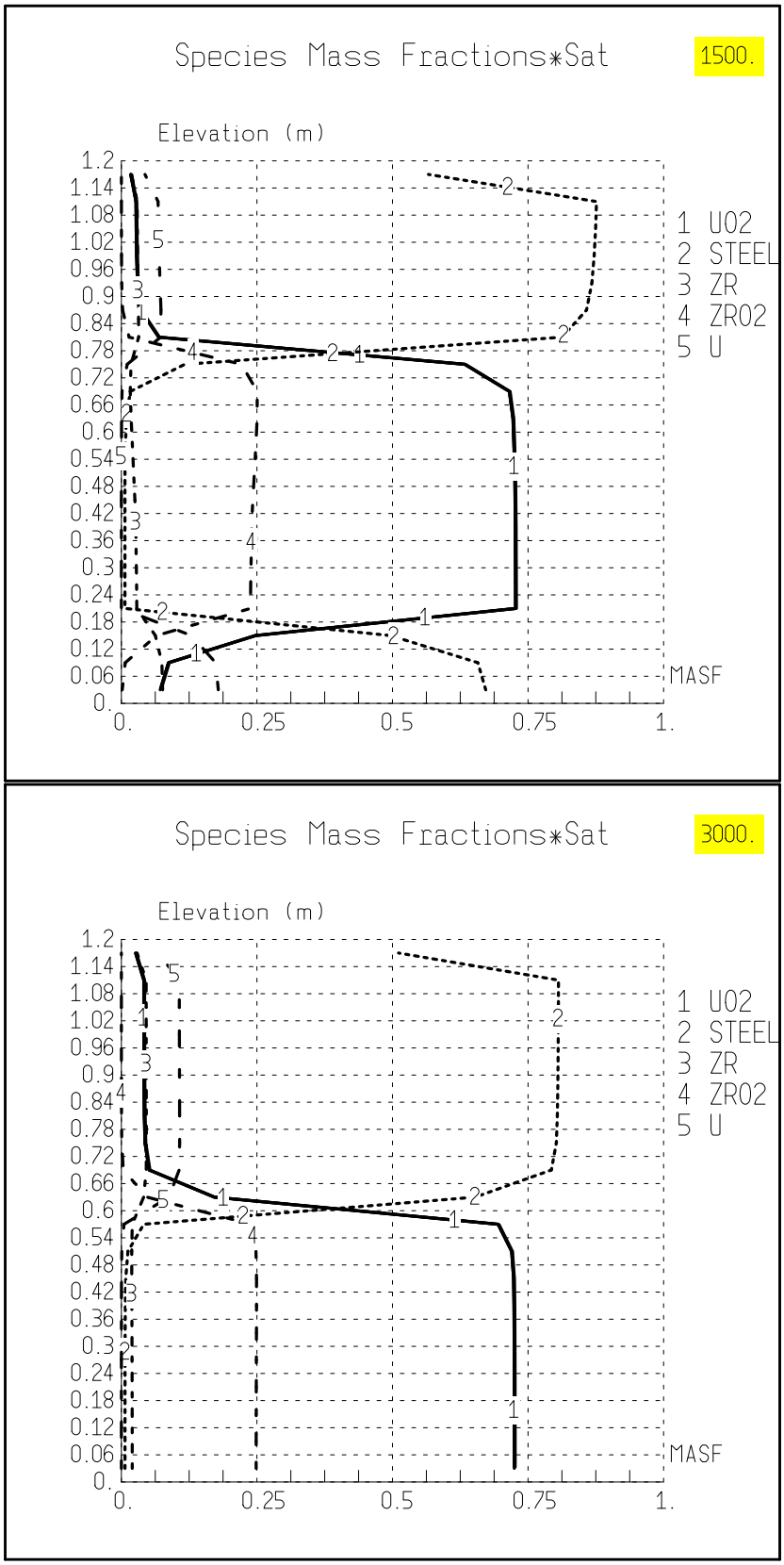

Fig. 11: Species concentration profiles B

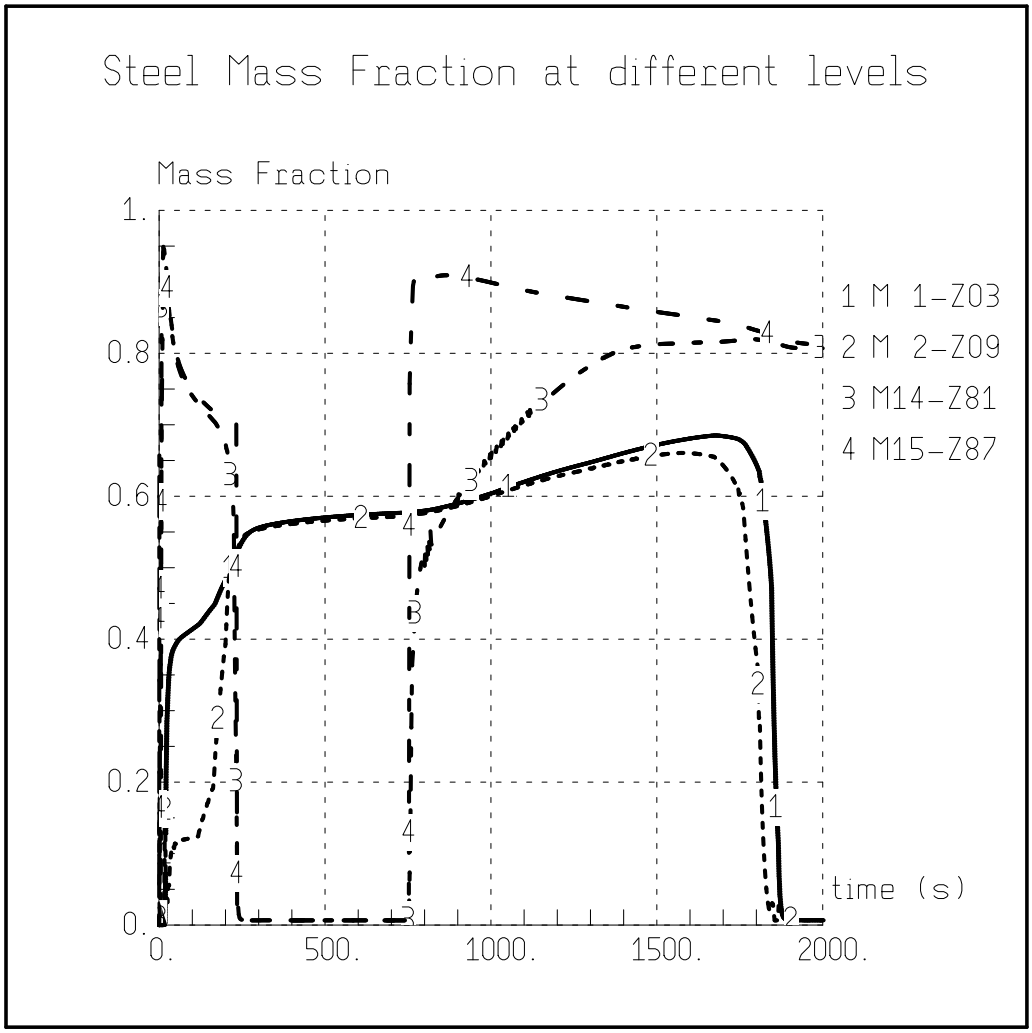

Fig. 12: Steel concentration history at selected elevations. 'M' designates mesh number and 'Z' the elevation of the center of the mesh (in cm)

Although the general behavior appears correct the inversion times shown in the plots may not be realistic because they are currently based on effective diffusivities which were arbitrarily set. Steel is plotted because it is a good indicator of the presence of the metallic phase. If significant amounts of steel are present the metallic phase is also present. It can be seen in the profiles that the corium level is approximately 0.8m after the initial steel injection (0-20s) and approximately 1.0m after the second injection (750-810s). The history plot contains four distinct intervals with a profile shown for each interval. The first interval, following the initial steel injection, is a 3 layer configuration. Around 250s the top metal layer becomes heavier than the oxide and sinks to the bottom joining the other layer. The steel injection (from the top) lasting from 750 to 810s creates another 3 layer configuration. A significant period of time after this second steel injection the lower metal layer becomes lighter than the oxide and floats to the top resulting in the final stable configuration.

There is a significant uncertainty in the residence time of the 3-layer configuration which, assuming that the chemical reactions are rather fast, will depend mainly on the rate of transport of free Uranium and Zirconium to this upper metal layer.
It can be seen in the history plot that:

- there is a gradual change in steel concentrations (and as a consequence layer density) within the metal layers when in an unstable configuration
- there is both a gradual change in the mixture levels within a layer when in an unstable configuration and also an abrupt change in the mixture levels during the inversions
- the switch from an unstable, 3-layer configuration to a stable 2-layer configuration occurs long after the steel injection
- the steel concentration in a mesh can be unstable when the physical system is in an unstable configuration (presumably due to slugs of metallic phase floating or sinking from one metal layer to the other).

Relative fission product mass profiles at the end of the run are shown for 12 selected fission products in Fig 13. Because injected steel does not contain fission products, their behavior is somewhat different than that of the main species. At 1500s the fission product concentration in the upper layer is very low.

6 2D application

6.1 PWR lower plenum transient

A lower head configuration was chosen as an illustration in real geometry of the operation and interaction of all transport models. The interaction between the one dimensional species transport model and the two dimensional species diffusion model (used to model mixing due to recirculation) are well shown. While the combination of diffusion and drift transport clearly are capable of predicting a stratified mixture in 2D the effects of corium recirculation, which are expected to be significant, are not accounted for. Buoyancy driven bulk flow recirculation was not calculated.
The evolution of phase stratification in a French PWR-900 lower head, initially at 750K, filled with approximately 50 tons of homogeneous UO_2, ZrO_2, Zr, and steel debris initially at a much higher temperature, 2500K, is simulated.
Although this is a simplified situation, these initial conditions could represent a situation immediately following debris arrival at the lower head in the event of negligible water presence or dry-out of the debris bed. The heat source, which is linearly proportional to the local (within a mesh) U content independent of chemical form, was chosen to illustrate the various physical phenomena affecting the corium such as the steel addition by melting of internal structures due to both radiation and convection, melting of the debris constituents at different temperatures with simultaneous refreezing of melt components in colder regions thereby constantly changing the overall local (and global) liquid corium composition, and thus, the local equilibrium phase compositions, phase

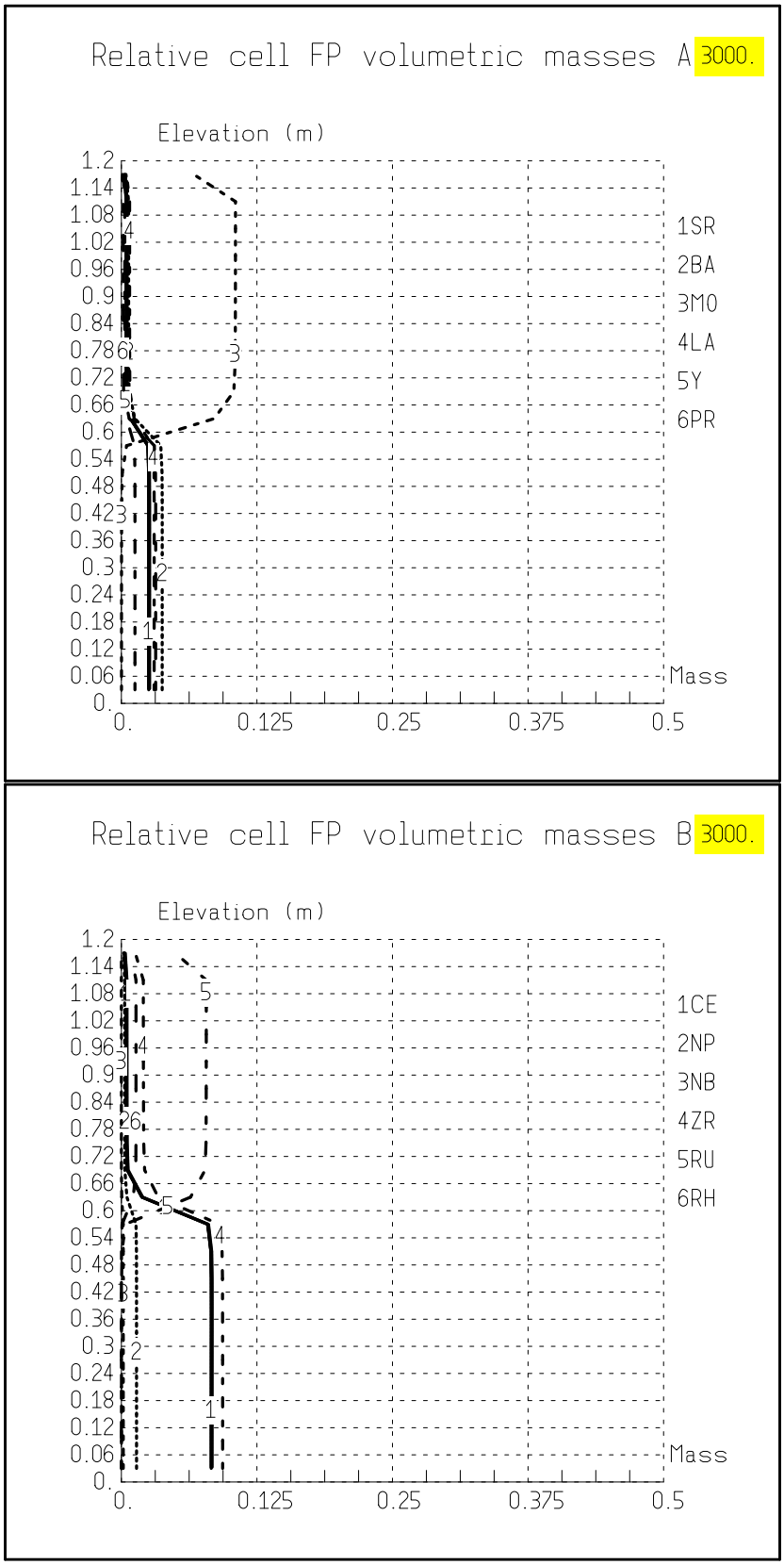

Fig. 13: Relative fission product profiles

densities, and even potentially switching the buoyant phase. For convenience, the lower head was supposed to be cooled on the outside by a flow of boiling water and was not allowed to fail.
Figs 14 and 15 show the steel concentration in the magma at selected times during the simulation. The parameter plotted is the steel mass fraction in the liquid (multiplied by the saturation) which serves as an indicator of the presence of the metallic phase. In this case the metal is the heavier phase during all the transient. The colormap was set to white for very small values to give an indication of the liquid level.
The simulation begins with a debris bed and intact internal steel structures. It ends with an oxide/metal stratified molten pool which contains most of the initial debris and the internal structures. It should be kept in mind that all freezing or melting alter the local liquid composition and also the local equilibrium phase compositions. The initial state for the simulation is shown in Fig. 14.
Throughout the simulation the debris bed rises in temperature and materials successively melt (steel, then Zr, $Zr0_2$ and finally UO_2. Debris near the plate structures stay relatively cold (near the fusion temperature of steel) until these structures are completely molten. The central region of the lower head remains colder than its surrounding until all debris melt. While this is not the expected result of a molten pool that begins at the central region, the deviation from expectation could result from a combination of the elevated volumetric heat source and large difference in temperature between debris and structures in the initial conditions.
Because the initial debris temperature is above the melting temperature of steel and Zirconium these are already in liquid form at the beginning of the simulation. Within the first 200s thin vertical steel rods/structures surrounded by debris have completely melted and added mass to the liquid while plates remain mostly intact. Although some of the liquid flows to the bottom of the lower head, much remains in the debris itself and the liquid/debris mix remains mostly uniform throughout the debris except for some materials that collect at the bottom and refreeze. At about 800s, the temperature in the bulk of the debris has reached the ZrO_2 fusion temperature adding the first oxides to the liquid. It is also with the melting of ZrO_2 that the debris field begins to lose its mostly homogenous liquid/solid mixture composition and divides into two distinct regions, a relatively liquid-free debris region and, beneath it, a liquid saturated debris region. This may be explained by the increased liquid saturation and the increased porosity (following ZrO_2 melting) which both contribute to a faster relocation of the liquid melt due to gravity. At this stage, it is interesting to notice that the metallic melt stays at the bottom but this is only because it fills the porosities between UO_2 particles, and despite the fact that it is lighter than UO_2. The size of the frozen steel region peaks around 1000s at which time the heat addition to this region from the debris begins to exceed the heat removal from this region to the lower head. This steel becomes liquid altering the local equilibrium compositions. This saturated debris configuration persists for a significant time with debris temperature increasing and plates melting, continuously adding steel to the liquid. The liquid metal/oxide stratification can be seen in the plot at 1400s, Fig. 14. The liquid free debris region temperature rises much faster than the liquid saturated debris region as less mass is available in the liquid free region to absorb the energy which is almost exclusively generated at this time in the

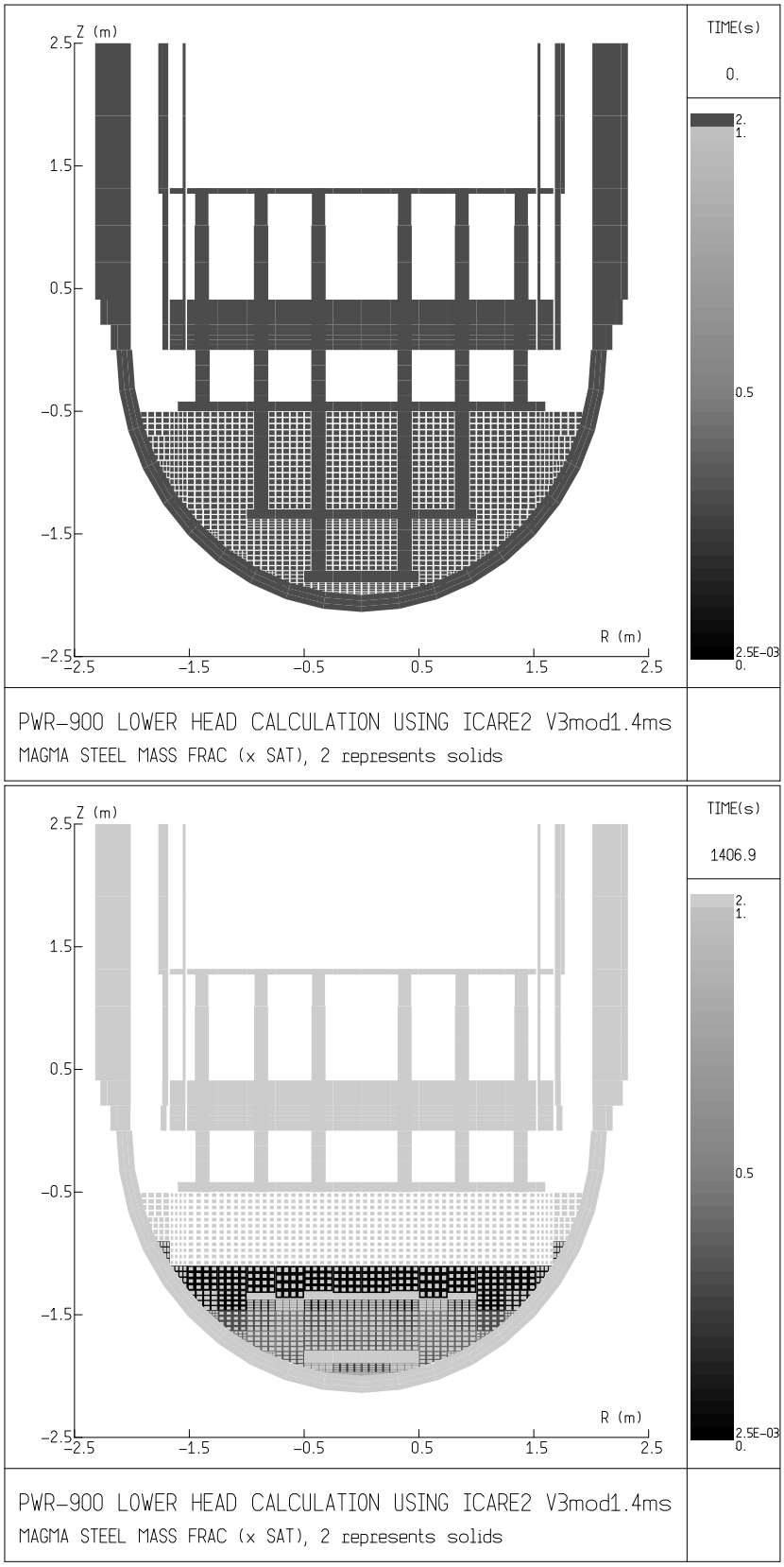

Fig. 14: Lower head steel concentrations A

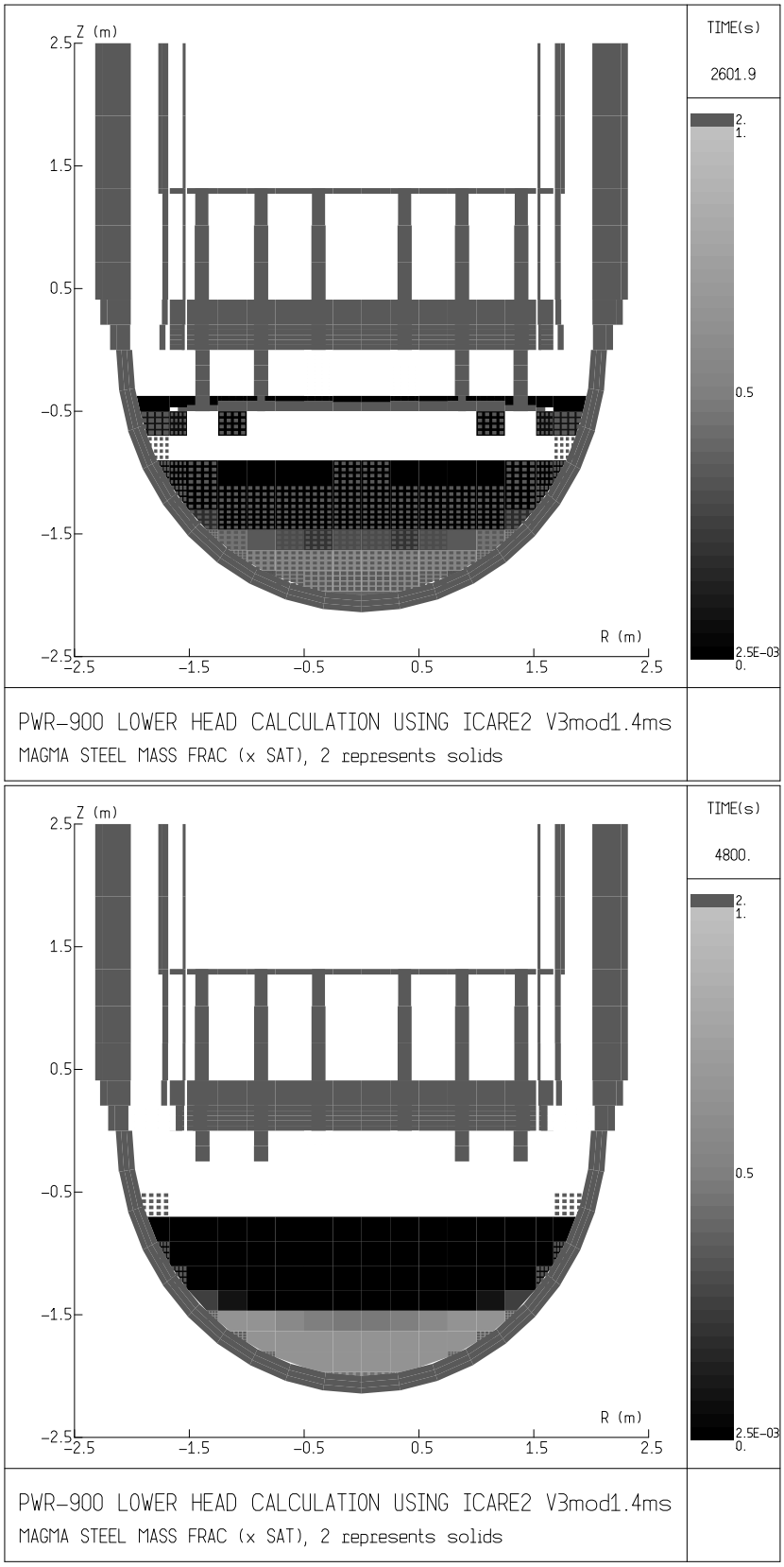

Fig. 15: Lower head steel concentrations B

solid UO_2. This temperature rise is relatively uniform throughout the liquid free region except for colder debris regions near the vessel wall. By 1800s the debris temperature has reached the metling temperature of UO_2 throughout the liquid free region except for near the vessel wall and for a slightly colder region near the plate directly above the debris. The support plate at an elevation of -1.3m has completely melted by this time. Large voids (cavities) develop in the liquid-free debris region by 2000s. The elevated debris temperatures results in an increase in radiative heat transfer to the upper structures which begin to melt near this time. The bottom plate at an elevation of -1.8m has completely melted by 2400s. By 2600s most of the liquid free debris region has melted. Some upper structures have melted and liquid steel has collected on the plate above the debris. The debris temperature in the liquid appears to have a vertical gradient. The UO_2 fusion temperature is reached at approximately the same time for the same elevation. It may be a consequence of the simultaneous metal/oxide stratification. The upper plate ruptures soon after 3000s and is completely melted by 3600s. The region occupied by debris shrinks from 2600s on until essentially none is left by 4000s. From 4000s on, the configuration consists of a metal/oxide stratified liquid field with a negatively buoyant metal phase. The final, stratified state at the end of the simulation at 4800s is shown in Figure 15.
Solid oxides were present throughout the entire simulation. The Oxygen potential of the liquid volume taken as a whole was always lower than the Oxygen potential of the initial debris.
This simulation shows the ability of the code to calculate the progressive melting and stratification in a two-dimensional lower plenum geometry. In the near future, different initial debris compositions will be selected to study the impact on stratification. In the present version of the code, the calculation of heat fluxes at the boundaries of stratified molten pools was not implemented. Therefore it is not yet possible to accurately estimate the transient heat fluxes along the vessel wall. This should be improved too.

7 Conclusions

A comprehensive model set involving both thermochemical and thermalhydraulic aspects has been developed to predict the stratification of oxides and metals in a corium pool. The model set is designed to be used on a 2D/3D meshing. Therefore, the corium pool is assumed to be non homogeneous in temperature and composition. Only local thermochemical equilibrium is assumed (in each mesh). A simplified thermochemical model provides the equilibrium compositions of the oxide and metallic phases. It is consistent with both MASCA experimental results and computational results obtained by using the IRSN thermochemical database. All the local physical properties, and particularly the densities, are calculated from the local compositions and temperature. The relative motion of the two phases is calculated with a drift flux model. This provides the velocities of the materials in the pool and, therefore, the global transport of species.
Fission products are also transported, assuming, for each fission product, a pre-defined local equilibrium distribution between oxide and metallic phases.

The model is implemented in a test-version of ICARE/CATHARE V2.0. Comparisons of the code results with selected MASCA tests show a good agreement.
The model set performs well in 0D/1D. It is possible to apply the 0D or 1D forms to lower head calculations depending on the level of modeling desired.
Reactor configurations have also been calculated, to study the effects of the progressive melting of lower plenum steel structures in a corium pool. The presented configuration has been selected to show the transient aspects of stratification. One advantage of this approach is the ability to deal with transient situations where the stratification may change according to the history of molten steel addition into the pool. The lower head model demonstrates that a transient 2D simulation on real geometry can be predicted using the developed model set involving changing debris composition, evolving corium composition, and a good description of the distribution of materials. Possible improvements have been identified for the different models. Some improvements are already under way, in particular for the thermochemical model and the efficiency of the numerical integration.
For the thermochemical models, one important improvement is the implementation of miscibility limits. Although this modification, which allows Oxygen in the metallic phase and steel in the oxidic phase, slightly deteriorates the prediction of the Uranium and Zirconium mass fractions in the metallic phase in the MASCA experiments, both the density of the metallic phase (due to the presence of UO_2 and/or ZrO_2) and the total mixture concentrations at which the density inversion occurs are improved. This is consistent with the current standard - Gibbs energy minimization calculations using current libraries which sometimes predict significant amounts of Oxygen in the metallic phase. It is necessary to be precise on the Oxygen quantity as the separation behavior is very sensitive to this parameter. Small differences in Oxygen mass fraction greatly change the predicted amount of Uranium and Zirconium in the metallic phase. Therefore, it is necessary to accurately predict corium oxidation by steam to accurately predict metal-oxide stratification. Up to now, MASCA experiments were performed in an inert environment. It is assumed that the reaction rate is limited by the molecular transport of free Zirconium to the interface, which means that the chemical reaction rate is much faster than the Zirconium transport. However, the present model assumes that the chemical equilibrium is always reached in every mesh, which is a much stronger assumption, and, it particular, it might lead to a meshing dependence. A transient chemistry may change the behavior, and the necessity to introduce it in the modelling will be checked.
The terminal velocity used is currently that of a single drop. This model should be changed to account for multiple drops or slugs. Making the drop size a function of the phase volume fraction (flow regimes) and turbulence (if modelled) would allow the calculation of emulsions and allow the calculation of increased relative phase velocities when larger drops (or slugs) are present.
Moreover, the potential surface tension reduction due to fission products that are soluble in both phases and that may collect at the interface has not been explored.
From a numerical point of view, the phase transport can be improved in two points:

- Determine the species redistribution in a different manner using new time species velocities instead new time species distribution

- Integrate phase separation into bulk flow calculation

Different applications to reactor configurations will be simulated to explore the possible transient configuration that might threaten the integrity of the vessel. The behavior will likely be different in a steam environment, specifically additional Zirconium oxidation by steam resulting in a reduction or cessation of Zirconium and Uranium migration to the metallic phase. If the molten pool is shielded from steam by a film or crust for a significant period of time the predicted behavior will be similar to the inert case. To be able to deal with a steam environment, a model for the molten pool oxidation will be introduced in ICARE/CATHARE.

Acknowledgments

The ICARE/CATHARE development and validation team is gratefully acknowledged for their help and support.

References

[1] V. G. Asmolov et al. The MA-2 experiment: Zirconium and uranium partitioning between oxide and metallic phases of molten corium. Technical Report MP-TR-6, Alexandrov Research Institute of Technology, 2002.

[2] V. G. Asmolov et al. Partitioning of fission products between the corium melt metallic and oxidic phases resulting from the STFM-FP tests. Technical Report MP-TR-10, Kurchatov Institute, 2003.

[3] Mehdi Baichi. *Contribution à l'étude du corium d'un réacteur nucléaire accidenté: aspects puissance résiduelle et thermodynamique des systèmes* $U - UO_2$ *et* $UO_2 - ZrO_2$. PhD thesis, 2001.

[4] S. Bechta. Results of the STFM Fe/MA experimental series and post-test analyses. In *MASCA 2002 Proceedings*, May 2002.

[5] W. Breitung and K.O. Reil. The density and compressibility of liquid (U,Pu)-mixed oxide. *Nucl. Sci. and Eng.*, 1990.

[6] J.A. Christensen. Thermal expansion and change in volume of uranium dioxide on melting. *Journal of American Ceramic Society*, 1963.

[7] R. Clift, J. R. Grace, and M. E. Weber. *Bubbles, Drops, and Particles*. Academic Press, 1978.

[8] CSNI/NEA. CSNI/NEA RASPLAV seminar 2000, summary and conclusions, Munich, Germany, 14-15 November 2000. Technical Report NEA/CSNI/R(2000)23, December 2000.

[9] W.D. Drotning. Thermal expansion of molten uranium dioxide. In *Proc. 8th Symposium On Thermophysical Properties ASME, II*, 1981.

[10] F. Fichot, V. Kobzar, Yu. Zvonarev, and P. Bousquet Mélou. The use of RASPLAV results in IPSN severe accident research program. In OECD-NEA, editor, *Proceedings of RASPLAV Seminar*, Munich, 2000.

[11] E.A. Fischer. Density of liquid uranium and derived equation state. Technical Report FZKA 6387, Forschungszentrum, 2000.

[12] A.V. Grosse, J.A. Cahill, and A.D. Kirschenbaum. *Journal of American Chemical Society*, (83):4665, 1961.

[13] V. Guillard, F. Fichot, P. Boudier, M. Parent, and R. Roser. ICARE/CATHARE coupling : three-dimensional thermalhydraulics of LWR severe accidents. In *Proceedings of ICONE 9,* 9^{th} *International Conference on Nuclear Engineering*, Nice Acropolis, France, April 2001.

[14] J.H. Harding and D.J. Martin. *J. Nucl. Mater*, (166):166, 1989.

[15] R.E. Henry and H.K. Fauske. External cooling of a reactor vessel under severe accident conditions. *Nuclear Engineering and Design*, 139:31–43, 1993.

[16] T. Iida and R.I.L. Guthrie. *The Physical Properties of Liquid Metals*. Clarendon Press Oxford, 1988.

[17] RRC Kurchatov Institute. Integrated report: Main results of the first phase of MASCA project, draft version. Technical report, RRC Kurchatov Institute, April 2004.

[18] Seiler J.-M. and Froment K. Material effects in late phases of severe accidents. *Multiphase Science and Technology*, 12:117–257, 2000.

[19] O. Kymalainen, H. Tuomisto, and T.G. Theofanous. In-vessel retention of corium at the loviisa plant. *Nuclear Engineering and Design*, 169:109–130, 1997.

[20] R.N.R. Mulford and R.I. Sheldon. Density and heat capacity of liquid uranium at high temperatures. *Journal of Nuclear Materials*, 1988.

[21] P.F. Paradis and W.K. Rhim. Thermophysical properties of zirconium at high temperature. *J. Mater. Res.*, 14(9), 1999.

[22] J.L. Rempe, D.L. Knudson, M. Cebull, and C.L. Atwood. Potential for in-vessel retention through ex-vessel flooding. *OECD/CSNI Workshop on In-Vessel Core Debris Retention and Coolability*, March 1998.

[23] W.G. Rohr and L.J Wittenberg. *Journ. Phys. Chem.*, (74):1151, 1970.

[24] Theerthan S.A., Kolb G., and Sehgal B.R. Heat transfer in internally heated liquid layers with stable stratification induced by phase separation. In *Proceedings of National Heat Transfer Conference*, August 2000.

[25] H. Tuomisto and T.G. Theofanous. A consistent approach to severe accident management. *Nuclear Engineering and Design*, 148:217–231, 1994.

A Thermochemical model equations

A.1 Separation calculations

The basic steps of the phase separation model are:

1. take U-Z-O-steel species from control volume
2. convert from total species masses to element mole fraction (i.e. n_U, n_Z, n_O, n_s)
3. perform calculations below to determine elemental separation into phases
4. convert from element mole fraction to species mass fraction for each phase assigning Oxygen first to U then Zr
5. convert from phase specific species mass fraction to total mesh species mass and fraction of each species in metallic phase - the second parameter indicates the fraction of each species that transports with each phase

Species masses are converted to element mole fractions. Steel is considered as an 'element'. Subsequently the following set of calculations is performed to determine the phasic separation:
Both the base model and miscibility limits are fits to calculations using the IRSN thermochemical database.
First the tie line is defined. Subsequently the tie line intersections with the metal and oxide miscibility limits are determined. If the initial concentration falls between the miscibility limits the mixture is considered to be immiscible and the concentrations calculated. Otherwise the mixture is considered to be miscible and all mass is assigned to the oxidic phase except for a residual of the same composition assigned to the metallic phase.
Given a mixture with U, Zr, O, and steel with mole fractions of n_U, n_Z, n_O, n_s, respectively:

$$
\begin{aligned}
Z_1 &= -1 + 4b - 3n_O + n_s + n_U + n_Z && (39)\\
Z_2 &= -1 + n_O - 3n_s + n_U + n_Z && (40)\\
b &= 0.5670 && (41)\\
m &= 0.09648 && (42)\\
F &= \frac{n_U}{n_U + n_Z} && (43)\\
& && (44)
\end{aligned}
$$

Unique position on tie line with no Oxygen content (UZsteel plane):

$$
\begin{aligned}
n_{snO} &= -\frac{Z_1 + mZ_2 - \sqrt{-16bmZ_2 + (Z_1 + mZ_2)^2}}{8m} && (45)\\
n_{UnO} &= (1 - n_{snO})F && (46)\\
n_{ZnO} &= (1 - n_{snO})(1 - F) && (47)\\
n_{OnO} &= 0 && (48)\\
& && (49)
\end{aligned}
$$

Unique position on tie line with no steel content (UZO plane):

$$\begin{aligned} n_{Ons} &= b + m n_{snO} && (50)\\ n_{Uns} &= (1 - n_{Ons})F && (51)\\ n_{Zns} &= (1 - n_{Ons})(1 - F) && (52)\\ n_{sns} &= 0 && (53) \end{aligned}$$

The initial model (i.e. without miscibility limit search) took the 'nO' values as the metallic phase composition and the 'ns' values as the oxidic phase composition as follows:

$$\begin{aligned} n_x &= n_O / n_{Ons} && (54)\\ n_m &= (1 - n_x) && (55)\\ n_{Um} &= (1 - n_{sno})F n_m && (56)\\ n_{Zm} &= (1 - n_{sno})(1 - F) n_m && (57)\\ n_{Om} &= 0 && (58)\\ n_{sm} &= n_{sno} n_m && (59)\\ n_{Ux} &= (1 - n_{Ons})F n_x && (60)\\ n_{Zx} &= (1 - n_{Ons})(1 - F) n_x && (61)\\ n_{Ox} &= n_{Ons} n_x && (62)\\ n_{sx} &= 0 && (63) \end{aligned}$$

If miscibilitiy limits were searched for the following operations are performed. The miscibility surface fit coefficients are as follows:

$$\begin{aligned} FM1 &= 0.0526256 && (64)\\ FM2 &= -0.0483533 && (65)\\ FM3 &= 0.590487 && (66)\\ FM4 &= -0.100888 && (67)\\ FM5 &= 0.0810992 && (68)\\ FM6 &= 0.09780439 && (69)\\ FX1 &= -.0546393 && (70)\\ FX2 &= .415816 && (71)\\ FX3 &= -.485481 && (72)\\ FX4 &= -.263494 && (73)\\ FX5 &= .38576 && (74)\\ FX6 &= .015707 && (75) \end{aligned}$$

The intersections of the miscibility surfaces with the tie line are iteratively solved for in the following manner using X_{FM} as a temporary variable indicating relative distance along the tie line from the no Oxygen UZs plane to no steel UZO plane:
Initial Guess for no steel mixture fraction:

$$X_{FM} = 0.5 \quad (76)$$

The following operations are performed 5 times to find the intersection of the tie line with metal miscibility limit:

$$
\begin{aligned}
D1 &= n_{UnO} - n_{UnO}X_{FM} + n_{Uns}X_{FM} && (77)\\
E1 &= n_{ZnO} - n_{ZnO}X_{FM} + n_{Zns}X_{FM} && (78)\\
F1 &= -n_{snO} - n_{UnO} + n_{Uns} && (79)\\
G1 &= -n_{ZnO} + n_{Zns} && (80)\\
A1 &= n_{snO} - n_{snO}X_{FM} + D1 && (81)\\
B1 &= A1 + E1 && (82)\\
C1 &= -F1 - G1 && (83)
\end{aligned}
$$

$$
FG = \frac{FM1 + \frac{E1FM2}{B1} + \frac{E1^2FM3}{B1^2} + \frac{D1FM4}{A1} + \frac{D1E1FM5}{A1B1} + \frac{D1^2FM6}{A1^2}}{n_{Ons}} - X_{FM} \qquad (84)
$$

$$
\begin{aligned}
DG = \; & \frac{1}{A1^3B1^3n_{Ons}}(-2B1^3D1^2F1FM6\\
& -A1B1^2D1(E1F1FM5 + B1(F1FM4 + 2FM6(n_{UnO} - n_{Uns})))\\
& +A1^2B1(-B1(B1FM4 + E1FM5)(n_{UnO} - n_{Uns})\\
& +D1FM5(B1G1 - E1(F1 + G1))) + A1^3(B1^2FM2G1 - B1^3n_{Ons}\\
& +2C1FM3(n_{ZnO} + G1X_{FM})^2\\
& +B1(2E1FM3G1 + C1FM2(n_{ZnO} + G1X_{FM})))) \qquad (85)
\end{aligned}
$$

$$
X_{FM}^{i+1} = X_{FM}^{i} - FG/DG \qquad (86)
$$

with 'i' indicating the iteration number.
The resultant X_{FM} after iterations is used to calculate the metallic phase specific concentrations. However, if X_{FM} is less than 0, it is reset to 0.

$$
\begin{aligned}
n_{Umm} &= X_{FM}n_{Uns} + (1 - X_{FM})n_{UnO} && (87)\\
n_{Zmm} &= X_{FM}n_{Zns} + (1 - X_{FM})n_{ZnO} && (88)\\
n_{Omm} &= X_{FM}n_{Ons} && (89)\\
n_{smm} &= (1 - X_{FM})n_{snO} && (90)
\end{aligned}
$$

For a smooth transition to a mixture where steel is immiscible with the rest of the mixture , a transition of the metallic phase surface is implemented:
If $n_{nsnO} \geq 0.85$ then the following calculations are made to adjust the metallic phase concentrations

$$
\begin{aligned}
xno &= \frac{n_{snO} - 0.85}{1 - 0.85} && (91)\\
n_{Umm} &= n_{UnO}xno + n_{Umm}(1 - xno) && (92)\\
n_{Zmm} &= n_{ZnO}xno + n_{Zmm}(1 - xno) && (93)\\
n_{Omm} &= n_{OnO}xno + n_{Omm}(1 - xno) && (94)\\
n_{smm} &= n_{snO}xno + n_{smm}(1 - xno) && (95)
\end{aligned}
$$

X_{FM} is reset to 0.5 as the initial guess for the oxidic phase. Then the following operations are performed 5 times to find the intersection of the tie line with oxide miscibility limit:

$$
\begin{aligned}
A2 &= (n_{UnO} + n_{ZnO})(1 - X_{FM}) + (n_{Uns} + n_{Zns})X_{FM} && (96)\\
B2 &= (n_{UnO} + n_{ZnO})(1 - X_{FM}) + (n_{Ons} + n_{Uns} + n_{Zns})X_{FM} && (97)\\
C2 &= n_{UnO} - n_{UnO}X_{FM} + n_{Uns}X_{FM} && (98)\\
D2 &= -n_{UnO} + n_{Uns} - n_{ZnO} + n_{Zns} && (99)
\end{aligned}
$$

$$
\begin{aligned}
FG &= -1 + X_{FM}\left(FX1 + \frac{C2FX4}{A2} + \frac{C2^2FX6}{A2^2} + \frac{FX2n_{Ons}X_{FM}}{B2}\right.\\
&\quad \left. + \frac{C2FX5n_{Ons}X_{FM}}{A2B2} + \frac{FX3n_{Ons}^2X_{FM}^2}{B2^2}\right)/n_{snO} && (100)
\end{aligned}
$$

$$
\begin{aligned}
DG &= 1 + \left(-\frac{C2D2FX4}{A2^2} - \frac{2C2^2D2FX6}{A2^3} + \frac{FX2n_{Ons}}{B2} + \frac{C2FX5n_{Ons}}{A2B2}\right.\\
&\quad + \frac{FX4(n_{Uns} - n_{UnO})}{A2} + \frac{2C2FX6(n_{Uns} - n_{UnO})}{A2^2} - \frac{C2D2FX5n_{Ons}X_{FM}}{A2^2B2}\\
&\quad + \frac{2FX3n_{Ons}^2X_{FM}}{B2^2} - \frac{FX2n_{Ons}(D2 + n_{Ons})X_{FM}}{B2^2}\\
&\quad - \frac{C2FX5n_{Ons}(D2 + n_{Ons})X_{FM}}{A2B2^2} + \frac{FX5n_{Ons}(n_{Uns} - n_{UnO})X_{FM}}{A2B2}\\
&\quad \left. - \frac{2FX3n_{Ons}^2(D2 + n_{Ons})X_{FM}^2}{B2^3}\right)/n_{snO} && (101)
\end{aligned}
$$

$$
X_{FM}^{i+1} = X_{FM}^{i} - FG/DG \qquad (102)
$$

with 'i' indicating the iteration number.
The resultant X_{FM} after iterations is used to calculate the oxidic phase specific concentrations. However, if X_{FM} is greater than 1, it is reset to 1.

$$
\begin{aligned}
n_{Uxx} &= X_{FM}n_{Uns} + (1 - X_{FM})n_{UnO} && (103)\\
n_{Zxx} &= X_{FM}n_{Zns} + (1 - X_{FM})n_{ZnO} && (104)\\
n_{Oxx} &= X_{FM}n_{Ons} && (105)\\
n_{sxx} &= (1 - X_{FM})n_{snO} && (106)
\end{aligned}
$$

A miscibility check is then made checking if the initial concentration falls between the metal and oxide concentrations. If the initial concentration does not fall in between, the mixture is considered miscible and all material is assigned to the oxidic phase except for a residual 10^{-15} of each element which is assigned to the metallic phase:

$$\begin{aligned} R &= 1 \times 10^{-15} && (107)\\ n_{Um} &= Rn_U && (108)\\ n_{Zm} &= Rn_Z && (109)\\ n_{Om} &= Rn_O && (110)\\ n_{sm} &= Rn_s && (111)\\ n_{Ux} &= (1-R)n_U && (112)\\ n_{Zx} &= (1-R)n_Z && (113)\\ n_{Ox} &= (1-R)n_O && (114)\\ n_{sx} &= (1-R)n_s && (115) \end{aligned}$$

If the mixture is found to be immiscible, then the following equations are used to give the molar concentrations in the control volume:

$$\begin{aligned} n_x &= (n_O - n_{Omm})/(n_{Oxx} - n_{Omm}) && (116)\\ n_m &= 1 - n_x && (117)\\ n_{Um} &= n_{Umm}n_m && (118)\\ n_{Zm} &= n_{Zmm}n_m && (119)\\ n_{Om} &= n_{Omm}n_m && (120)\\ n_{sm} &= n_{smm}n_m && (121)\\ n_{Ux} &= n_{Uxx}n_x && (122)\\ n_{Zx} &= n_{Zxx}n_x && (123)\\ n_{Ox} &= n_{Oxx}n_x && (124)\\ n_{sx} &= n_{sxx}n_x && (125) \end{aligned}$$

For each phase the updated element mole fractions are converted to species mass fraction assuming that Oxygen is associated first to Uranium, then to Zirconium.
The heat of reaction for the chemical reaction is calculated so that the temperature remains unchanged.

A.2 Range of Validity

For an Oxygen to Uranium and Zirconium mole ratio greater than approximately 1.97 the predicted fraction of steel in the metallic phase exceeds 1. This matches the conditions when MASCA data shows no Uranium or Zirconium in the metallic phase. If this occurs (i.e. $n_{snO} \geq 1$), the metallic phase is considered to consist of solely steel and the oxidic phase is considered to consist of everything else. The phase concentrations are the same as for the miscible case except for:

$$\begin{aligned} n_{sm} &= (1-R)n_s && (126)\\ n_{sx} &= Rn_s && (127) \end{aligned}$$

B Terminal velocity equations

The terminal velocity is adapted from a model presented in Clift, Grace, and Weber [7] for contaminated systems of single drops in infinite media which is considered to be valid for the following ranges:

$$\begin{aligned} \mathrm{M} &< 10^{-3} && (128)\\ \mathrm{Eo} &< 40 && (129)\\ \mathrm{Re} &> 0.1 && (130) \end{aligned}$$

Additional constraints are there due to the presence of wall effects in the form of drop diameter to hydraulic diameter ratio. Hydraulic diameters are expected to be very large (unless, of course, a mesh contains both corium and solid debris)
The Eo number using the maximum drop size limitation is 16. For anything smaller Eo is also smaller.
The largest possible Morton number is calculated using possible extremes for the species in question:

$$\begin{aligned} \mathrm{M}_{\max} &= \frac{g\mu_{\max}^4 \Delta\rho_{\max}}{\rho_{\min}^2 \sigma_{\min}^3} && (131)\\ &\approx \frac{10 \times 0.0225^4 \times 10,000}{6,000^2 \times 1.8^3} && (132)\\ &\approx 1.2 \times 10^{-10} && (133) \end{aligned}$$

The Re using this method were found to be sufficiently large (> 1000) for the expected density differences. The maximum drop diameter increases more rapidly than the velocity decrease (for both metallic phase and oxidic phase drops) resulting in increasing Reynolds number with decreasing density difference. This model is applied to both dispersed metallic and oxidic phases. The final calculated terminal velocity is a volume fraction weighted combination of the two forcing the value to go to zero as either volume fraction goes to zero.
The terminal velocity equations are as follows: Drop diameters:

$$\begin{aligned} \Delta\rho &= |\rho_m - \rho_x| && (134)\\ d_m &= 4\sqrt{\frac{\sigma_m}{g\Delta\rho}} && (135)\\ d_x &= 4\sqrt{\frac{\sigma_x}{g\Delta\rho}} && (136) \end{aligned}$$

This formulation is approximately the maximum stable bubble drop when the drop viscosity is greater than half the viscosity of the continuous fluid. This may not be the case with oxide drops in a mostly steel metallic phase due to higher steel viscosity.

Morton and Eötvös numbers:

$$\mathrm{M}_m = \frac{g\mu_x^4\Delta\rho}{\rho_x^2\sigma_m^3} \quad (137)$$

$$\mathrm{M}_x = \frac{g\mu_m^4\Delta\rho}{\rho_m^2\sigma_x^3} \quad (138)$$

$$\mathrm{Eo}_m = \frac{g\Delta\rho d_m^2}{\sigma_m} \quad (139)$$

$$\mathrm{Eo}_x = \frac{g\Delta\rho d_x^2}{\sigma_x} \quad (140)$$

For $d = d_{\max}$, Eo = 16.
Two parameters, H and J, defined in the model have a linear relationship in two different ranges - i.e. there was a different relationship between H and J for H less than 59.3 and for H greater than 59.3. This point is the approximate point at which oscillatory drop behavior begins thus changing the terminal velocity behavior. Because it was found that for typical corium properties H is always much greater than 59.3 only the applicable J relationship is shown (and used).

$$\mathrm{H}_m = \frac{4}{3}\mathrm{Eo}_m\mathrm{M}_m^{-0.149}\left(\frac{\mu_x}{\mu_w}\right)^{-0.14} \quad (141)$$

$$\mathrm{H}_x = \frac{4}{3}\mathrm{Eo}_x\mathrm{M}_x^{-0.149}\left(\frac{\mu_m}{\mu_w}\right)^{-0.14} \quad (142)$$

$$\mathrm{J}_m = 3.42\mathrm{H}_m^{0.441} \quad (143)$$

$$\mathrm{J}_x = 3.42\mathrm{H}_x^{0.441} \quad (144)$$

μ_w was given as $0.0009\mathrm{Km}^{-1}\mathrm{s}^{-1}$.
The terminal velocities for each phase assuming each is the dispersed phase are then calculated as:

$$u_{t,m} = \frac{\mu_x}{\rho_x d_m}\mathrm{M}_m^{-0.149}(\mathrm{J}_m - 0.857) \quad (145)$$

$$u_{t,x} = \frac{\mu_m}{\rho_m d_x}\mathrm{M}_x^{-0.149}(\mathrm{J}_x - 0.857) \quad (146)$$

The final mesh terminal velocity is then taken as:

$$u_t = (u_{t,m}\alpha_x + u_{t,x}\alpha_m)/\mu_r \quad (147)$$

where μ_r is the relative viscosity (dimensionless) which takes into account possible solid debris particles flowing with the corium.